Kinetic approach to modelling CO_2 adsorption from humid air using amine-functionalized resin

Elfving, Jere; Sainio, Tuomo

Published in:
Chemical Engineering Science

DOI:
10.1016/j.ces.2021.116885

Published: 31/12/2021

Document Version
Publisher's final version

Chemical Engineering Science 246 (2021) 116885

Contents lists available at ScienceDirect

Chemical Engineering Science

journal homepage: www.elsevier.com/locate/ces

Kinetic approach to modelling CO_2 adsorption from humid air using amine-functionalized resin: Equilibrium isotherms and column dynamics

Jere Elfving [a,*], Tuomo Sainio [b]

[a] VTT Technical Research Centre of Finland Ltd., Koivurannantie 1, FI-40101 Jyväskylä, Finland
[b] Lappeenranta-Lahti University of Technology, School of Engineering Science, Mukkulankatu 19, 15210 Lahti, Finland

HIGHLIGHTS

- Kinetic model for CO_2 adsorption from humid air on amine-functionalized adsorbent.
- Humid CO_2 adsorption isotherms modelled using the kinetic model.
- Enhancement of CO_2 capacity by humidity captured well by isotherm modelling.
- Dynamic model fitted to fixed-bed data in humid direct air capture conditions.
- Non-isothermal adsorption of CO_2 and H_2O reproduced well by the dynamic model.

GRAPHICAL ABSTRACT

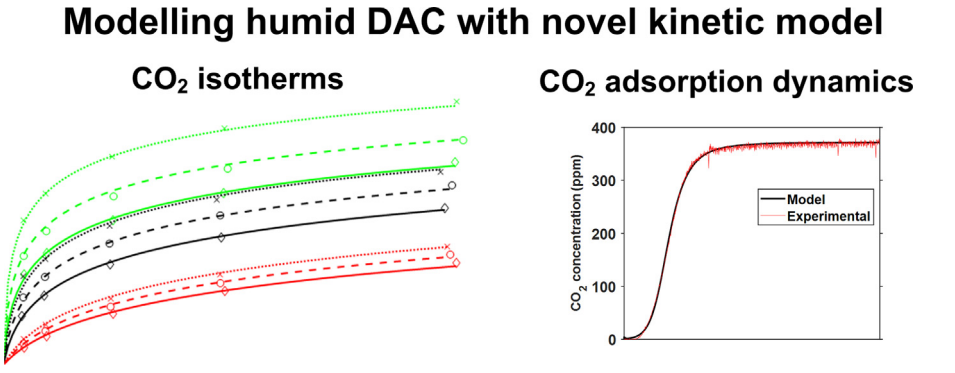

ARTICLE INFO

Article history:
Received 22 March 2021
Received in revised form 14 June 2021
Accepted 15 June 2021
Available online 22 June 2021

Keywords:
Direct air capture
CO_2 adsorption
H_2O adsorption
Co-adsorption
CO_2 isotherms
Kinetic model

ABSTRACT

Humidity can up to double the adsorption capacity of CO_2 in conditions relevant to direct air capture (DAC) on amine-functionalized adsorbents, but the treatment of this phenomenon in isotherm or kinetic models has been all but neglected in the literature. In this work, a kinetic model based on reaction mechanisms of CO_2 adsorption on supported amines in dry and humid conditions is proposed. The kinetic model was used in modelling of humid CO_2 adsorption isotherms and dynamics of fixed-bed CO_2 adsorption from air. The improvement of equilibrium CO_2 capacity by humidity was captured well by the kinetic model, leading to good fits of CO_2 isotherms. At best, the dynamic model closely represented the whole shape of CO_2 adsorption breakthrough curves in several-hour fixed-bed adsorption experiments. Therefore, the proposed kinetic model is expected to be useful in simulation of the DAC process based on supported amine-adsorbents.

1. Introduction

To not exceed the global warming targets of 1.5 °C or 2 °C by the end of the century requires sharp reduction of global CO_2 emissions to net zero in the coming decades. Any credible scenarios that can meet these targets require not only CO_2 emission reduction via technologies such as post-combustion capture (PCC), but also the use of carbon removal technologies, among which is capturing CO_2 directly from air. (Coninck et al., 2018) Direct air capture (DAC) usually involves the use of strongly basic solutions or solid sorbents to selectively capture CO_2 from air, followed by the release of CO_2 from the solvent or sorbent in a concentrated form via heating, pressure swing, humidity swing or other methods

* Corresponding author.
E-mail address: jere.elfving@vtt.fi (J. Elfving).

https://doi.org/10.1016/j.ces.2021.116885
0009-2509/

(Sanz-Pérez et al., 2016). As a result, the DAC process can produce pure CO_2 carbon negatively, although the carbon efficiency of DAC is largely dependent on the carbon footprint of the electricity and heat used (de Jonge et al., 2019; Deutz and Bardow, 2021). DAC coupled with carbon storage (DACCS) could reach carbon removal of several Gt_{CO2}/a scale (Breyer et al., 2019; Fuss et al., 2018). On the other hand, DAC can also be combined with different CO_2 utilization technologies (DACCU). DACCU enables a fully renewable energy system by using the produced CO_2 for chemical energy storage in power-to-X (PtX) technologies such as the Fischer-Tropsch process, while producing carbon–neutral fuels for the transport sector (Vidal Vázquez et al., 2018). Another use of DAC is to boost food production in greenhouses (Rodríguez-Mosqueda et al., 2019) or in microbial cultivation (Ruuskanen et al., 2021).

While DAC utilising hydroxide solvents may be an efficient technology for large-scale operation (Keith et al., 2018) and in terms of cost is comparable to solid sorbent technology (Fasihi et al., 2019), it is also a fairly complex process with heat demands that cannot be supplied by low-grade waste heat. One type of sorbent-based DAC is the humidity-swing process which utilizes anion-exchange resins, and entails the advantage of sorbent regeneration in atmospheric conditions (Shi et al., 2017; Van Der Giesen et al., 2017). However, water demand during the regeneration phase may limit the geographical applicability of this technology (Van Der Giesen et al., 2017). By contrast, DAC based on amine-functionalized adsorbents does not require water, instead humidity in air is captured, and thus liquid water can be produced (Bajamundi et al., 2019). This process only requires a temperature near 100 °C or less for sorbent regeneration, which enables the use of low-grade waste heat (Bajamundi et al., 2019; Wurzbacher et al., 2016), and can be assembled as scalable modular units (Climeworks, 2021). The adsorbents combine the CO_2-selective amine groups with porous materials such as mesoporous silica, alumina or metal–organic framework (MOF) via impregnation of polyamines, grafting of aminosilanes or surface-initiated polymerization of amines (Sanz-Pérez et al., 2016; Shi et al., 2020).

The co-adsorbed water can be both a nuisance and an advantage in CO_2 capture from air. Co-adsorbed humidity may increase the adsorbent regeneration heat requirement several times compared to dry case with only CO_2 adsorbing (Drechsler and Agar, 2020). Although the energy penalty related to water can be minimized via e.g. heat recovery (Drechsler and Agar, 2020), it is important to be able to evaluate the amount of co-adsorbed H_2O via measuring H_2O isotherms such as in (Veneman et al., 2015; Gebald, 2014). Another negative implication of humidity can be adsorbent degradation, which can occur for example in some metal–organic frameworks (MOFs) (Jahandar Lashaki et al., 2019). On the other hand, humidity may increase the CO_2 adsorption capacity due to a change in the reaction mechanism between CO_2 and amine groups.

Capture of CO_2 in a primary or secondary amine-functionalized adsorbent in dry conditions takes place via formation of an intermediate zwitterion, which can be stabilized by a basic group, such as a neighbouring amine or a water molecule (Sanz-Pérez et al., 2016; Choi et al., 2009; Li et al., 2016). In the case of one primary amine group reacting with CO_2, the formation of the zwitterion can be written as:

$$CO_2 + NH_2 - R \underset{k_b}{\overset{k_f}{\rightleftharpoons}} RNH_2^+COO^- \quad (1)$$

In dry conditions, the zwitterion is deprotonated by a neighbouring amine group, resulting in the formation of ammonium carbamate:

$$RNH_2^+COO^- + NH_2 - R \underset{k_{b,1}}{\overset{k_{f,1}}{\rightleftharpoons}} RNHCOO^- : RNH_3^+ \quad (2)$$

Therefore, in dry conditions, two moles of amine are required to capture one mole of CO_2.

However, the evidence of which species is formed under humid conditions is ambiguous in the literature. For tertiary amines, formation of bicarbonate in humid conditions has been proposed, while in dry conditions tertiary amines cannot capture CO_2 at all (Choi et al., 2009; Lee et al., 2017). For primary and secondary amines, the formation of bicarbonate in humid conditions has also been proposed based on infrared (Didas et al., 2014) and NMR studies (Chen et al., 2018). The formation of bicarbonate from the zwitterion with primary amines in humid conditions would take place via:

$$RNH_2^+COO^- + H_2O \underset{k_{b,2}}{\overset{k_{f,2}}{\rightleftharpoons}} RNH_3^+ : HCO_3^- \quad (3)$$

However, based on the quantum chemical model by (Li et al., 2016), the mechanism of CO_2 capture in humid conditions more likely leads to hydronium carbamate than bicarbonate:

$$RNH_2^+COO^- + H_2O \underset{k_{b,2}}{\overset{k_{f,2}}{\rightleftharpoons}} RNHCOO^- : H_3O^+ \quad (4)$$

Hahn et al. (2015) also proposed the formation of a water-stabilized carbamate species based on NMR data. Also, Yu and Chuang (2017)) observed the formation of both carbamic acid and hydronium carbamate in humid or wet CO_2 adsorption on tetraethylenepentamine (TEPA) film via in-situ FTIR. Whichever the reactions in Eqs. (3) or (4) or the formation of water-stabilized carbamic acid take place in humid conditions, the result is that only one amine group is required per mole of CO_2, which theoretically boosts the maximum available CO_2 capacity up to double that of dry conditions.

The increase of CO_2 capacity in humid DAC conditions has been reported for different amine-functionalized adsorbents. For a nanofibrillated cellulose (NFC) adsorbent grafted with aminosilanes, Gebald (2014) reported adsorption capacities of 1.11 and 2.13 $mmol_{CO2}/g_{sorbent}$ at 23 °C using dry and humid (2.5 vol-% H_2O) 400 ppm CO_2, respectively. The improvement of capacity due to humidity was even more heavily promoted at 50 °C, with 0.11 and 1.42 $mmol_{CO2}/g_{sorbent}$ in dry and humid conditions, respectively. Sayari et al. (2016) found that CO_2 capacity increased with increasing relative humidity (RH) on pore-expanded MCM-41-supported PEI adsorbent, with the highest capacity of 2.92 $mmol_{CO2}/g_{sorbent}$ achieved at 64% RH, marking a 34% improvement compared to dry conditions (2.18 $mmol_{CO2}/g_{sorbent}$). Kumar et al. (2020) used SBA-15 impregnated with 60 w-% of alkyl-aryl amine groups to measure CO_2 capacities of 1.6 and 2.9 $mmol_{CO2}/g_{SiO2}$ from 400 ppm CO_2 at 35 °C in dry and 30% RH conditions, corresponding to over 81% capacity improvement in humid conditions. For the adsorbent used in this work, CO_2 capacities using 400–5000 ppm CO_2 were 0.54–0.92 $mmol_{CO2}/g_{sorbent}$ in dry conditions, and 0.89–1.28 $mmol_{CO2}/g_{sorbent}$ with around 63% RH at 25 °C (Elfving et al., 2017). The improvement of CO_2 capacity by humidity was thus 65% at 400 ppm and 39% at 5000 ppm CO_2. Moreover, based on isotherm modelling, humidity increased the attainable working capacities by up to around 80% in the temperature-swing regeneration process at an adsorption temperature of 25 °C.

However, in some cases, only marginal improvement or even a decrease of capacity in humid conditions has been reported. For example, (Goeppert et al., 2011) reported a capacity increase from 1.18 to 1.77 $mmol_{CO2}/g_{sorbent}$ in dry and humid (67% RH) conditions for a 33 w-% PEI-loaded fumed silica adsorbent, but with 50 w-% PEI loading, the same experiment resulted in a decrease of capacity from 1.7 to 1.41 $mmol_{CO2}/g_{sorbent}$. Also, Wang et al. (2015) measured only modest improvement of CO_2 capacity on a 55 w-% PEI-loaded mesoporous carbon adsorbent from 2.25 to 2.58 $mmol_{CO2}/g_{sorbent}$ from dry 400 ppm CO_2 and with 80% RH, respec-

tively. On the other hand, sometimes the improvement in humid conditions is more than the theoretical maximum of doubling of the capacity. Sujan et al. (2019) reported only 0.59 $mmol_{CO2}/g_{sorbent}$ under dry conditions but 1.6 $mmol_{CO2}/g_{sorbent}$ with 85% RH from 400 ppm CO_2 at 35 °C for a 41 w-% PEI-impregnated silica-fiber adsorbent. Also, although not in DAC conditions, Qi et al. (2014) obtained a remarkable capacity of 11.8 $mmol_{CO2}/g_{sorbent}$ from 8% CO_2 at 25 °C with 18% relative humidity, but only 0.82 $mmol_{CO2}/g_{sorbent}$ in dry conditions in a two-hour experiment. These results impart that, in some cases, the effect of humidity on CO_2 capacity is explained by a change of CO_2 adsorption kinetics rather than a change in equilibrium capacity. In adsorbents with high loading of amine, adsorbed water could act as an additional barrier for diffusion of CO_2 (Hahn et al., 2015; Si et al., 2019), but on the other hand, humidity could also enhance the flexibility of amino-polymer chains and thus enhance gas diffusion (Qi et al., 2014; Kolle et al., xxxx).

Despite the significant effect of humidity on the capacity and possibly the kinetics of CO_2 adsorption from air on amine-based adsorbents, few attempts have been made to model this phenomenon. Although binary isotherm models for describing competitive CO_2/H_2O adsorption systems have been reported, e.g., Langmuir with Brunauer-Emmett-Teller (BET) (Wang et al., 2020), these models cannot be used to model CO_2/H_2O adsorption on amine-based adsorbents. The enhancing effect of humidity on CO_2 capacity requires a different approach to isotherm modelling. Wurzbacher et al. (2016) used Toth isotherms measured in dry conditions coupled with an enhancing factor to take into account the effect of humidity on CO_2 capacity. However, the factor was determined from only four measurements using bilinear interpolation, instead of co-adsorption isotherm modelling. Their data was later used by Stampi-Bombelli et al. (2020) to describe the CO_2 adsorption from air in humid conditions using a modified Toth model that takes into account the enhancing effect of humidity. In their model, two additional parameters are introduced, which, combined with H_2O capacity, increase the adsorption affinity and CO_2 maximum capacity under humid conditions. While this approach seems fairly straightforward, only a few isotherm points were reported, and it was not assessed how accurately this model could depict the co-adsorption isotherms.

Another approach to humid CO_2 adsorption modelling on amine-functionalized adsorbents was presented by Jung and Lee (2020), who used the reaction mechanisms of CO_2 and H_2O with amines as a basis to describe the reaction rate equations of CO_2 to carbamate and bicarbonate. In their rate equations, the reaction stoichiometry was neglected, and the reactions have separate maximum capacities, which would mean that two different sites of CO_2 adsorption exist in the adsorbent. Moreover, they used these rate equations as a basis to derive a temperature-dependent co-adsorption isotherm model for CO_2, which resembles the dual-site Langmuir isotherm. They fitted this model to CO_2/H_2O co-adsorption points at 40–70 °C, and showed fairly good representation of the equilibrium data by the model. However, in their data, the CO_2 capacity was lower in humid conditions at CO_2 partial pressures below 0.15 bar at 40–55 °C. Also, the partial pressures of both CO_2 and H_2O were 0.025 bar or higher, so it could not be deduced how well the proposed model depicts lower partial pressure levels or DAC conditions. Therefore, more work is required on finding models that can accurately describe the enhancing effect of humidity on CO_2 adsorption in adsorbent-based DAC.

In this work, a kinetic model based on the kinetics of adsorption and desorption reactions is proposed for CO_2 adsorption from air on amine-functionalized resin. The model includes different mechanisms of CO_2 adsorption in dry and humid conditions on amine-functionalized adsorbents. The model is used to describe adsorption equilibrium isotherms by integrating until equilibrium. Parameters describing adsorption equilibrium are fitted to (pseudo-)equilibrium CO_2 isotherms measured in humid conditions. The kinetic model is then used in the dynamic simulation of fixed-bed adsorption column to fit mass and heat transfer parameters from experimental CO_2 and H_2O breakthrough curves and temperature data. Adsorption equilibrium of H_2O in the simulation is calculated by the Guggenheim Anderson De Boer (GAB) model fitted to experimental single-component H_2O isotherms. To the authors' best knowledge, this is the first time that an adsorption mechanism-based model has been used to accurately describe the equilibrium and kinetics of CO_2 adsorption in humid DAC conditions.

2. Experimental and modelling methods

2.1. CO_2/H_2O adsorption experiments

In this study, an automated and modifiable fixed-bed adsorption device was used in experimental work. Details of the experimental setup have been previously reported in (Elfving et al., 2021). Approximately 0.5 g of a proprietary amine-functionalized resin characterized in (Elfving et al., 2017) was fixed in the column with quartz wool below and above the adsorbent. All experiments were conducted using the temperature-vacuum-concentration swing adsorption (TVCSA) process described in detail below. The samples were first regenerated by temperature-concentration swing (TCS) and vacuum (TVCS) to remove pre-adsorbed CO_2 and H_2O. Regeneration was done with 1000 ml/min of N_2 during TCS and 100 ml/min during TVCS, with a vacuum level of around 50 mbar. The dry weight of the sample used for capacity calculations was gained by subtracting the mass of the pre-adsorbed species from the mass measured before inserting the sample into the column.

Regeneration was followed by CO_2 adsorption using humidified compressed air or 200–4000 ppm CO_2 obtained by mixing 1% CO_2/N_2 and N_2. The gases were humidified using the moisture calibrator Hovacal digital 122-SP. For single-component H_2O isotherms pure N_2 was used as the balance gas, and was humidified similarly as the humid CO_2/N_2 mixtures. Adsorption was carried out for four hours at 25–50 °C. To allow convenient automatic measurement of the single-component H_2O isotherms, H_2O concentrations from 0.16 to 1.86 vol-% were obtained by varying the total flow rate of N_2 from 1000 to 100 ml/min, respectively, while keeping the moisture calibrator set-point constantly at 0.2 vol-%.

The CO_2/H_2O co-adsorption isotherm points were measured at 5 concentrations of CO_2 between 200 and 4000 ppm, at 25–50 °C, and with 3 concentrations of H_2O, the set-points in the moisture calibrator being 0.2 vol-%, 1 vol-% and 2 vol-% H_2O. Each isotherm consisted of 5 consequent adsorption/desorption cycles where the CO_2 partial pressure was varied and temperature and H_2O concentration were kept constant. The sample was changed for each isotherm. The adsorption time for the co-adsorption isotherm experiments was 5–6 h. The flow rate for the first two co-adsorption isotherms (0.2 vol-% H_2O, 25 °C and 35 °C) was only 200 ml/min, but to make sure the CO_2 adsorption was near saturation, the flow rate in the consequent experiments was kept at 500 ml/min. However, even at 25 °C, the difference between the CO_2 capacities gained using 0.2 vol–% H_2O and 200 ml/min were not significantly lower than those measured at 500 ml/min (see Supplementary Data Fig. S1). Therefore, the two CO_2 isotherms with 0.2 vol-% H_2O at 25 °C and 35 °C measured using 200 ml/min flow rate were used with other isotherms measured using 500 ml/min in the modelling of humid CO_2 adsorption isotherms.

The actual measured concentrations of CO_2 and H_2O were different from the set-points, and for H_2O they were on average

0.16 vol-%, 0.95 vol-% and 1.9 vol-%. However, the variation in the concentrations did not add to the uncertainty of the isotherm points, since partial pressures were used in the isotherm models instead of concentration. The partial pressures p_i of the CO_2 and H_2O isotherm points were calculated by the measured molar fractions y_i (step function concentrations) and column average pressure P_{tot} during adsorption using $p_i = P_{tot}y_i$. The partial pressures of H_2O in the humid CO_2 isotherms for the three humidity set-points of 0.2 vol-%, 1 vol-% and 2 vol-% were in the range of 0.0016–0.0017 bar, 0.0098–0.0103 bar and 0.0185–0.0205 bar, respectively.

The adsorption phase was followed by complete desorption of the adsorbed species. The desorption phase consisted of purging with N_2 at 1000 ml/min, temperature swing up to 100 °C and vacuuming with 100 ml/min N_2 purge. To find the effect of co-adsorption on water capacity, the experiments with 0.2 vol-% H_2O were run with separate purge steps for CO_2 and H_2O by first stopping the CO_2 flow ('Purge 1'), and then using dry N_2 ('Purge 2'). A slight peak in H_2O concentration during 'Purge 1' was noted in some cases, but the method was deemed too uncertain due to integration of the small peak against the noisy H_2O concentration. The capacities gained this way were in the range of below zero up to only 0.036 $mmol_{H2O}/g_{sorbent}$. Therefore, in consequent experiments, the purge steps were combined.

The cyclic humid experiment was done with two-hour adsorption phases using CO_2 and H_2O concentration set-points of 400 ppm and 2 vol-% at 25 °C and a total flow rate of 1000 ml/min. The desorption phase was similar to the one in the co-adsorption experiments. Furthermore, a single experiment with a nearly two-day adsorption phase was done where humidified compressed air with 2 vol-% H_2O and 401 ppm CO_2 was used at a flow rate of 100 ml/min. The calculation of CO_2 and H_2O capacities is discussed in the Supplementary Data. Experimental repeatability was calculated as trend uncertainty from the cyclic experiment (see Section 3.1), being ± 0.200 $mmol_{H2O}/g_{sorbent}$ and ± 0.092 $mmol_{H2O}/g_{sorbent}$ for the H_2O adsorption and desorption capacities, respectively. For adsorption and desorption of CO_2, the repeatability was ± 0.009 $mmol_{CO2}/g_{sorbent}$ and ± 0.010 $mmol_{CO2}/g_{sorbent}$, respectively. A more detailed description of uncertainty with the current experimental device can be found in earlier work (Elfving et al., 2021).

2.2. Isotherm and kinetic models

The temperature-dependent Toth model (Do, 1998) has been used for modelling the adsorption of CO_2 on amine-functionalized solid adsorbents (Veneman et al., 2015; Gebald, 2014; Elfving et al., 2017; Serna-Guerrero et al., 2010), but also for water adsorption on porous adsorbents (Wang and LeVan, 2009; Qasem and Ben-Mansour, 2018). However, the Toth isotherm lacks the multilayer adsorption behaviour encountered in porous adsorbents such as nanofibrillated cellulose (Gebald, 2014; Stampi-Bombelli et al., 2020) or polystyrene-based resin (Veneman et al., 2015) that have been functionalized with amines. For describing the H_2O adsorption on amine-functionalized adsorbents, the Brunauer Emmett Teller (BET) (Drechsler and Agar, 2020) and the GAB (Gebald, 2014) isotherms have been used. However, the typical form of BET model has no temperature dependency. Therefore, the GAB-isotherm is used in this work to model H_2O adsorption on the aminoresin:

$$q_{H2O} = \frac{q_{m,mono} C K (p_{H2O}/p_{H2O,sat})}{(1 - K(p_{H2O}/p_{H2O,sat})(1 + K(p_{H2O}/p_{H2O,sat})(C-1))} \quad (5)$$

where q_{H2O} is the H_2O adsorption capacity at partial pressure p_{H2O} and water saturation vapour pressure of $p_{H2O,sat}$ and $q_{m,mono}$ is the monolayer adsorption capacity of H_2O. Parameters C and K are temperature-dependent:

$$C = C_0 \exp\left(\frac{\Delta H_C}{R_{id} T}\right) \quad (6)$$

$$K = K_0 \exp\left(\frac{\Delta H_K}{R_{id} T}\right) \quad (7)$$

where C_0 and K are dimensionless parameters and ΔH_C and ΔH_K are adsorption enthalpies of monolayer and multilayer adsorption. (Gebald, 2014; Stampi-Bombelli et al., 2020; Sultan et al., 2015; Quirijns et al., 2005) Because ΔH_C can be expected to be positive and ΔH_K negative (Sultan et al., 2015; Quirijns et al., 2005), the lower boundary of ΔH_C and the upper boundary of ΔH_K were fixed at zero during isotherm fitting.

Based on reactions presented in Eqs. (1)–(4), the adsorption rates of CO_2 in dry and humid conditions can be described with the following equations:

$$r_1 = k_{f,1}[\text{R-NH}_2]^2[CO_2] - k_{b,1}[\text{RNHCOO}^- : \text{RNH}_3^+] \quad (8)$$

$$r_2 = k_{f,2}[\text{R-NH}_2][CO_2][H_2O] - k_{b,2}[\text{RNHCOO}^- : H_3O^+] \quad (9)$$

where k_f and k_b are the kinetic constants of forward and backward reactions, respectively. Square brackets refer to the concentrations of the respective reaction species. Subscripts 1 and 2 refer to the reactions in dry and humid conditions, respectively. Although the rate Eq. (9) for reaction 2 shows the formation of hydronium carbamate in humid conditions (Eq. (4)), another option is bicarbonate formation (Eq. (3)), as discussed above. Similarly to (Jung and Lee, 2020), the amine species concentration [R-NH_2] is the solid-phase concentration of available amine sites for adsorption of CO_2, while the concentrations of CO_2 and H_2O are replaced with the respective partial pressures. Also, the product concentrations [$RNHCOO^-$:RNH_3^+] and [$RNHCOO^-$:H_3O^+] are replaced with the solid-phase concentrations of CO_2 of $q_{1,CO2}$ and $q_{2,CO2}$, i.e. the CO_2 adsorption capacity for reactions 1 and 2, respectively. However, contrary to (Jung and Lee, 2020), the available amine sites concentration is here calculated from balance q_m-$2q_{1,CO2}$ -$q_{2,CO2}$, with common maximum capacity of amine sites q_m being available for both reactions. In other words, reaction 1 consumes two amine sites per mole of CO_2, and reaction 2 consumes only one amine site per mole of CO_2. The backward reaction rate constant can be written in terms of the adsorption affinity b as $k_b = k_f/b$. Therefore, the resulting mass balance equations are written as:

$$\frac{dq_{1,CO2}}{dt} = k_{f,1}(q_m - 2q_{1,CO2} - q_{2,CO2})^2 p_{CO2} - \frac{k_{f,1}}{b_1} q_{1,CO2} \quad (10)$$

$$\frac{dq_{2,CO2}}{dt} = k_{f,2}(q_m - 2q_{1,CO2} - q_{2,CO2}) p_{CO2} p_{H2O} - \frac{k_{f,2}}{b_2} q_{2,CO2} \quad (11)$$

The total rate of change in CO_2 adsorption $dq_{tot,CO2}/dt$ is then calculated by a sum of the reaction rate Eqs. (10) and (11). The adsorption affinity is temperature-dependent:

$$b_1 = b_{0,1} \cdot \exp\left(\frac{-\Delta H_1}{R_{id} \cdot T_0} \cdot \left(\frac{T_0}{T} - 1\right)\right) \quad (12)$$

$$b_2 = b_{0,2} \cdot \exp\left(\frac{-\Delta H_2}{R_{id} \cdot T_0} \cdot \left(\frac{T_0}{T} - 1\right)\right) \quad (13)$$

where $b_{0,1}$ and $b_{0,2}$ are the reference adsorption affinities at reference temperature T_0, while $-\Delta H_1$ and $-\Delta H_2$ are the opposite numbers of isosteric heats of adsorption for reactions 1 and 2, respectively.

Eqs. (10) and (11) coupled with the temperature dependency of the adsorption affinity are referred to later in this work as the 5-

parameter co-adsorption model. In this model, the exponents of the available amine site concentration in reactions 1 and 2 originate from the reaction stoichiometry.

It is also possible to fit these exponents from experimental data. Denoting the exponents by t_1 and t_2 gives:

$$\frac{dq_{1,CO2}}{dt} = k_{f,1}\left(q_m - 2q_{1,CO2} - q_{2,CO2}\right)^{t_1} p_{CO2} - \frac{k_{f,1}}{b_1} q_{1,CO2} \quad (14)$$

$$\frac{dq_{2,CO2}}{dt} = k_{f,2}\left(q_m - 2q_{1,CO2} - q_{2,CO2}\right)^{t_2} p_{CO2} p_{H2O} - \frac{k_{f,2}}{b_2} q_{2,CO2} \quad (15)$$

Eqs. (12)–(15) are in this work referred to as the 7-parameter co-adsorption model. The 5-parameter and 7-parameter co-adsorption models were used to model the CO_2 adsorption kinetics in humid conditions.

The co-adsorption models were fitted to all the humid CO_2 desorption isotherm data at 25–50 °C to find equilibrium parameters q_m, b_1, b_2, $-\Delta H_1$, $-\Delta H_2$, and additionally t_1 and t_2 in the case of the 7-parameter model. Given sufficient time, the equilibrium state is determined by the *ratio* of forward and backward rate constants rather than their absolute values. Therefore, the forward kinetic parameters can be set to arbitrary values (here $k_{f,1} = k_{f,2} = 1$) while ensuring that the equilibrium state is reached by integrating long enough in time. At a later stage, the forward kinetic parameters can be estimated from kinetic data by using the previously determined values for the equilibrium parameters. In this work, dynamic CO_2 breakthrough data was used to estimate the kinetic constants by using the fixed-bed model, as described in the next section.

To calculate the total equilibrium CO_2 capacity when fitting the models to CO_2 isotherms, the kinetic models were integrated for a sufficiently long time to reach equilibrium using the 'ODE15s' -solver in Matlab. The relative and absolute tolerances for the ODE solver 'RelTol' and 'AbsTol' were $1{\cdot}10^{-10}$. The isotherm fitting for both single-component H_2O GAB isotherms and the co-adsorption models was done by using the 'lsqnonlin' -optimization function with termination tolerances 'Tolfun' and 'TolX' of $1{\cdot}10^{-10}$. To help find global minima, the 'MultiStart' function in Matlab was utilized for the fitting of the H_2O isotherms with 100 starting points, while for the 5-parameter model, 50 starting points were used. In the case of the 7-parameter model, the fitted parameters of the 5-parameter model were used as the starting points.

2.3. Fixed-bed adsorption column model

A dynamic model was written for non-isothermal co-adsorption of CO_2 and H_2O in a column packed with the amine-functionalized resin. Mass and heat balance equations along the axial direction of the bed were solved by using the method of lines in Matlab. Ideal gas law was used for gas phase calculations such as calculating partial pressures from concentrations. Since this work only considers the adsorption phase and low concentrations of CO_2 and H_2O, gas velocity along the bed is constant in this model. Possible adsorption of N_2 or O_2 from compressed air is not taken into account due to non-existent or negligible competition with CO_2 or H_2O due to physical adsorption mechanism, near atmospheric pressure (see Table 1) and the low surface area of the resin of 32 m^2/g (Elfving et al., 2017). Moreover, the total pressure is constant in the model, since the effect of the pressure drop along the bed on partial pressures of CO_2 and H_2O was assumed to be negligible. For example, in experiments with a 500 ml/min total flow rate, the average pressure drop across the bed during adsorption was 230 Pa at 25 °C and 180 Pa at 35 °C with 2 vol-% H_2O and around 370 ppm CO_2. Thermal equilibrium between the solid and gas phases was assumed. Bed properties such as voidage, adsorbent density and specific heat capacity are constant. Also, case-dependent thermodynamic properties of the gas such as kinematic viscosity, gas density and specific heat capacity were calculated for the inlet gas in each case based on gas composition, total pressure and temperature, but are constant within each simulation case. The solid phase and gas phase properties as well as initial and boundary conditions can be found in Table 1.

Table 1
Parameters used in the fixed-bed modelling. NIST database values were obtained with the 'refpropm'- user-built function in Matlab and REFPROP software using corresponding inlet gas composition, temperature and total pressure.

Quantity	Parameter	Value	Source
	Adsorbent bed properties		
L_{bed}	Bed length	0.017–0.018 *m*	Calculated from column dimensions and bulk density
R_{bed}	Bed radius	0.0045 *m*	Column inner radius
ϵ	Bed voidage	0.375	Adsorbent SDS
ρ_B	Bulk density	450 kg/m^3	Measured
R_p	Particle radius	$3{\cdot}10^{-4}$ *m*	From particle size distribution median (Elfving et al., 2017)
ρ_p	Particle density	720 kg/m^3	Calculated from voidage and bulk density
$c_{p,a}$	Specific heat capacity of adsorbent	1580 J/(kg K)	From (Sonnleitner et al., 2018). Resin matrix similar type.
	Inlet gas properties		
$y_{CO2,feed}$	Feed molar fraction of CO_2	0.00037–0.00040	Measured
$y_{H2O,feed}$	Feed molar fraction of H_2O	0.0016–0.0193	Measured
T_{feed}	Feed gas temperature	298–308 K	Set equal to measured bed temperature
ρ_g	Gas mixture density	1.13–1.20 kg/m^3	NIST database
v_i	Interstitial velocity	0.070–0.349 m/s	Calculated from flow rate and voidage
ν	Kinematic viscosity of gas mixture	1.48–$1.61{\cdot}10^{-5}$ m^2/s	NIST database
$c_{p,CO2}$	Molar heat capacity of CO_2	851–861 J/(mol K)	NIST database
$c_{p,H2O}$	Molar heat capacity of H_2O	4180 J/(mol K)	NIST database
$c_{p,g}$	Specific heat capacity of gas mixture	1050–1060 J/(kg K)	NIST database
	Process conditions		
T_w	Column wall temperature	298–308 K	Set equal to measured bed temperature
P_{tot}	Total pressure in the column	1.03–$1.07{\cdot}10^5$ Pa	Measured

The component material balance can be represented as:

$$\frac{\partial c_i}{\partial t} = D_L \frac{\partial^2 c_i}{\partial z^2} - v_i \frac{\partial c_i}{\partial z} - \frac{\rho_B}{\varepsilon} \frac{\partial q_i}{\partial t} \quad (16)$$

where c_i is the concentration of species i, t is time, D_L is the axial dispersion coefficient, z is axial dimension, v_i is the interstitial velocity, ρ_B is the adsorbent bed bulk density and ε is the bed porosity (Bollini et al., 2012; Shafeeyan et al., 2014; Haghpanah et al., 2013). Several correlations exist for calculating the axial dispersion coefficient, but here the Chung & Wen correlation was used:

$$D_L = \frac{2R_p v_i \varepsilon}{0.2 + 0.011 Re^{0.48}} \quad (17)$$

where R_p is the adsorbent particle radius and Re is the Reynold's number calculated by $Re = 2R_p v_i \varepsilon / \nu$, where ν is the kinematic viscosity of the inlet gas mixture (Rastegar and Gu, 2017). The kinetics of total CO_2 adsorption arise from the sum of Eqs. (10) and (11) or (14) and (15), as explained above. However, as the adsorption of H_2O was described with the GAB isotherm model, the linear driving force model (Sircar and Hufton, 2000) was used to describe the water adsorption kinetics:

$$\frac{d\bar{q}_i}{dt} = k_{i,\mathrm{LDF}}(q_{i,\mathrm{eq}} - \bar{q}_i) \tag{18}$$

where $\bar{q}_i$ is the average capacity of species i in the adsorbent particle, $k_{i,\mathrm{LDF}}$ is the linear driving force kinetic constant and $q_{i,\mathrm{eq}}$ is the equilibrium capacity of species i, arising from the isotherm model. Specifically, in the fixed-bed model $q_{i,\mathrm{eq}}$ is the local equilibrium capacity depending on the partial pressure of species i and temperature in the gas arriving to the given grid point at time t.

The heat balance is a simplified form of the model used by Haghpanah et al. (2013) in that gas velocity and pressure are constant. Also, in this work, there is no separate heat balance at the column wall, since the wall temperature along radial and axial directions was assumed to be uniform. The heat balance takes into account convection and dispersion along the axial direction of the bed, sensible heat of the adsorbed molecules, exothermic heat of adsorption and heat transfer between the bed and the column wall:

$$\begin{aligned}&\frac{1-\varepsilon}{\varepsilon}\rho_p\left(c_{p,a} + c_{p,\mathrm{CO2}}\cdot q_{\mathrm{tot,CO2}} + c_{p,\mathrm{H2O}}\cdot q_{\mathrm{H2O}}\right)\frac{\partial T}{\partial t}\\ &= \frac{K_z}{\varepsilon}\frac{\partial^2 T}{\partial z^2} - \rho_g c_{p,g} v_i \frac{\partial T}{\partial z} - \frac{1-\varepsilon}{\varepsilon}\rho_p\left(c_{p,\mathrm{CO2}}\frac{dq_{\mathrm{tot,CO2}}}{dt} + c_{p,\mathrm{H2O}}\frac{dq_{\mathrm{H2O}}}{dt}\right)T\\ &\quad - \frac{1-\varepsilon}{\varepsilon}\rho_p\left(-\Delta H_1\frac{dq_{1,\mathrm{CO2}}}{dt} + (-\Delta H_2)\frac{dq_{2,\mathrm{CO2}}}{dt} + (-\Delta H_{\mathrm{Toth}})\frac{dq_{\mathrm{H2O}}}{dt}\right) - \frac{2h}{\varepsilon R_{\mathrm{bed}}}(T - T_w)\end{aligned} \tag{19}$$

where ρ_p is the adsorbent particle density, $c_{p,a}$ is the specific heat capacity of the adsorbent, $c_{p,\mathrm{CO2}}$ and $c_{p,\mathrm{H2O}}$ are the molar heat capacities of CO_2 and H_2O, respectively, K_z is the axial effective heat conductivity, ρ_g is the gas density, $c_{p,a}$ is the specific heat capacity of the gas, h is the overall heat transfer coefficient between the bed and the column wall, R_{bed} is the adsorbent bed radius and T_w is the wall temperature.

At the inlet boundary, the Danckwert's boundary condition was used:

$$D_L\left.\frac{\partial c_i}{\partial z}\right|_{z=0} = -v_i(c_{i,\mathrm{feed}} - c_i|_{z=0}) \tag{20}$$

where $c_{i,\mathrm{feed}}$ is the feed concentration of species i, and $c_i|_{z=0}$ is the concentration of species i at the column inlet boundary. At the outlet boundary, the boundary condition is:

$$\left.\frac{\partial c_i}{\partial z}\right|_{z=L} = 0 \tag{21}$$

where L is bed length. Analogously for the heat balance, the inlet boundary condition (Haghpanah et al., 2013; Farooq and Ruthven, 1990) is:

$$K_z\left.\frac{\partial T}{\partial z}\right|_{z=0} = -\varepsilon v_i \rho_g c_{p,g}(T_{\mathrm{feed}} - T|_{z=0}) \tag{22}$$

and the outlet boundary condition:

$$\left.\frac{\partial T}{\partial z}\right|_{z=L} = 0 \tag{23}$$

As for initial conditions, the adsorbent bed is regenerated ($q_{\mathrm{H2O}} = 0$; $q_{\mathrm{CO2,1}} = 0$; $q_{\mathrm{CO2,2}} = 0$; $q_{\mathrm{CO2,tot}} = 0$) and emptied from adsorbing species ($c_{\mathrm{CO2}} = 0$; $c_{\mathrm{H2O}} = 0$), temperature in the column is equal to column wall and inlet gas temperature ($T = T_w = T_{\mathrm{feed}}$). Discretization of the ODEs was done via finite difference method. Details of the discretization can be found in Supplementary Data.

As mentioned above, the desorption isotherm data of CO_2 and H_2O was corrected by empty column desorption capacities, which was then used for fitting the equilibrium parameters of the CO_2 kinetic model (Eqs. (10)–(15)) and the GAB model parameters for H_2O. Therefore, when using these models in the dynamic fixed-bed model, the simulated adsorption breakthrough curves would lead to an early breakthrough in comparison to the measured adsorption breakthrough curves. For CO_2 near 400 ppm, this is not significant (see Supplementary Data of (Elfving et al., 2021)), but for H_2O, the effect of the empty column needs to be accounted for in the model. Therefore, empty column adsorption capacities were measured at several H_2O concentrations, and a Langmuir isotherm model was fitted to this data. The capacity calculated from this model was added to the H_2O equilibrium capacity in Eq. (18). The model fit and parameters are shown in Supplementary Data Fig. S2.

The fixed-bed model was fitted to scaled dynamic experimental data to find parameters $k_{f,1}$, $k_{f,2}$, $k_{\mathrm{H2O,LDF}}$, K_z and h. The used experimental data was CO_2 and H_2O breakthrough curves and the temperature of the bed measured approximately 1 cm into the bed. The data fitting was done by using the Matlab function "lsqcurvefit" with termination tolerances 'FunTol' and 'TolX' of $1{\cdot}10^{-8}$ and $1{\cdot}10^{-10}$. The number of control volumes in all simulations was 200. Equations for scaling the data are found in the Supplementary Data.

3. Results & discussion

3.1. Humid cyclic experiment

Earlier, only dry cyclic experiments (Elfving et al., 2021) have been done with the resin studied in this work. Therefore, to find the capacity decrease rate and repeatability in humid conditions, a cyclic TVCSA run with 2 vol-% H_2O and 370–380 ppm CO_2 was done, and the results are shown in Fig. 1. Fig. 1a shows good agreement of cyclic adsorption and desorption capacities, with difference of the two falling below 0.02 $\mathrm{mmol_{CO2}/g_{sorbent}}$. However, Fig. 1c shows that the H_2O adsorption capacities are clearly higher than the desorption capacities by 0.29–0.93 $\mathrm{mmol_{H2O}/g_{sorbent}}$. The main reasons for this difference probably lie in humidity sensor accuracy (±1% RH) and additional uncertainty related to calculating the H_2O adsorption capacities, which is discussed in more detail in Supplementary Data (Calculation of experimental capacities).

The CO_2 adsorption and desorption capacities decreased from around 0.87 $\mathrm{mmol_{CO2}/g_{sorbent}}$ to 0.77 $\mathrm{mmol_{CO2}/g_{sorbent}}$ and 0.76 $\mathrm{mmol_{CO2}/g_{sorbent}}$ in 17 cycles, respectively. The exact capacity drops corresponded to 11.1% and 12.4% or 0.65%/cycle and 0.73%/-cycle for adsorption and desorption, respectively. Meanwhile, the H_2O desorption capacities decreased from 3.82 to 2.96 $\mathrm{mmol_{H2O}/g_{sorbent}}$, which corresponds to a 22.6% drop, or 1.33%/cycle. In earlier work (Elfving et al., 2021), the greatest CO_2 capacity drop found in dry conditions of 0.60%/cycle was gained when using temperature-vacuum swing adsorption with air purge at 100 °C, being on similar scale to the results above. On the other hand, the capacity drop in dry conditions using TCS regeneration was only 0.18%/cycle (Elfving et al., 2021). Since the regeneration in the humid cyclic experiment was conducted using dry gases, and the resin was mostly dry by the time temperature swing was started, leaching of amines by moisture should not be the cause of the capacity drops. It can be observed from Fig. 1b and 1d that in the last 5–6 cycles the capacities seem to stabilize. This could refer to the least stable amine sites being deactivated or removed first, causing the initial rapid decrease of capacity. On the other

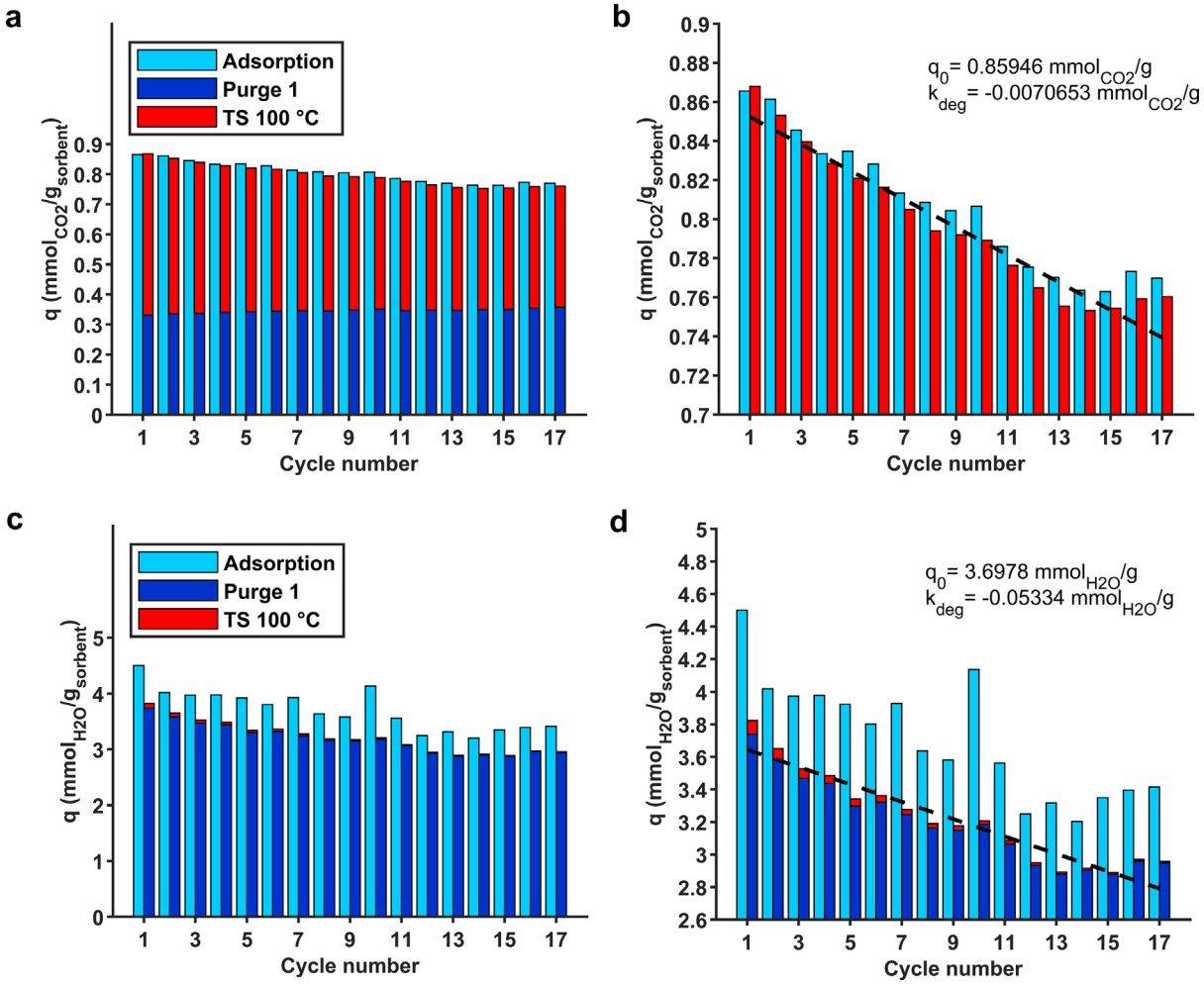

Fig. 1. CO_2 and H_2O adsorption and desorption capacities in repeated cycles of temperature-concentration-vacuum swing adsorption. Sub-figures b) and d) are close-ups from a) and c), respectively, and show the linear fit and parameters to total desorption capacities.

hand, this could also be due to the regeneration method not being fully complete, leaving small amounts of CO_2 and H_2O adsorbed after each cycle until cyclic steady-state is reached. This could be due to more stable species formed between CO_2 and amines under humid adsorption conditions, as suggested by infrared spectroscopy studies (Yu and Chuang, 2017; Miller et al., 2020). However, the real reason for the capacity drop rates requires further investigation in future work.

Regardless of the reason for the capacity drops, the implication for the isotherm results is the same, and requires data correction. Fig. 1b and 1d show a linear fit to the desorption capacities of CO_2 and H_2O with coefficients of determination of 0.94 and 0.90, respectively. Although the capacity drops are not linear for the last cycles, these linear functions give an estimate of the capacity drop rate for CO_2 and H_2O in humid conditions. Therefore, this data was used to correct the isotherm point data below as described in Supplementary Data (equation S1).

3.2. H_2O isotherms

Fig. 2 shows the experimental H_2O desorption data and the GAB isotherm fit gained for the amine-functionalized polystyrene resin. The isotherm data in Fig. 2a shows that at 35 °C and 50 °C, the H_2O capacity progresses almost linearly with increasing partial pressure. However, at 25 °C, the isotherm shows a type III isotherm shape, corresponding to multilayer H_2O adsorption. Similar behaviour of H_2O adsorption on amine-functionalized adsorbents has been reported for, e.g., Lewatit VP OC 1065 (Veneman et al., 2015) and aminosilane-functionalized NFC (Gebald, 2014). Fig. 2b shows that the H_2O isotherms seem to be a function of relative humidity rather than both temperature and relative humidity. However, as data was not gathered from the total relative humidity range due to the risk of water condensation in the experimental device lines, it was "safer" to use the temperature-dependent GAB model.

Table 2 shows the GAB isotherm parameters. For the heat balance of the fixed-bed model, the isosteric heat of adsorption was calculated at zero loading via $-\Delta H_{H2O,0} = \Delta H_C + \Delta H_K + \Delta H_{H2O,vap}$ (Gebald, 2014; Sultan et al., 2015; Quirijns et al., 2005), where $\Delta H_{H2O,vap}$ is the heat of H_2O vaporization of 44.1 kJ/mol$_{H2O}$, resulting in 50.7 kJ/mol$_{H2O}$. Another method to estimate the isosteric heat of adsorption is from the Clausius Clapeyron equation by fitting $\ln(p_{H2O})$ derived from GAB isotherm vs. $1/T$ (see e.g. (Sultan et al., 2015)), resulting in 50.1 kJ/mol$_{H2O}$ near zero loading (1E-6 mmol$_{H2O}$/g$_{sorbent}$). These values are comparable with, e.g., 43 kJ/mol$_{H2O}$ for Lewatit VP OC 1065 (Veneman et al., 2015) and 48.8 kJ/mol$_{H2O}$ for amine-functionalized NFC (Gebald, 2014). Thus, the adsorption enthalpy of −50.7 kJ/mol$_{H2O}$ is used in the heat balance of the dynamic model in this work.

Fig. 2 also shows H_2O desorption capacities from the co-adsorption isotherm experiments where 370–380 ppm CO_2 was adsorbed simultaneously. These points are in good agreement with

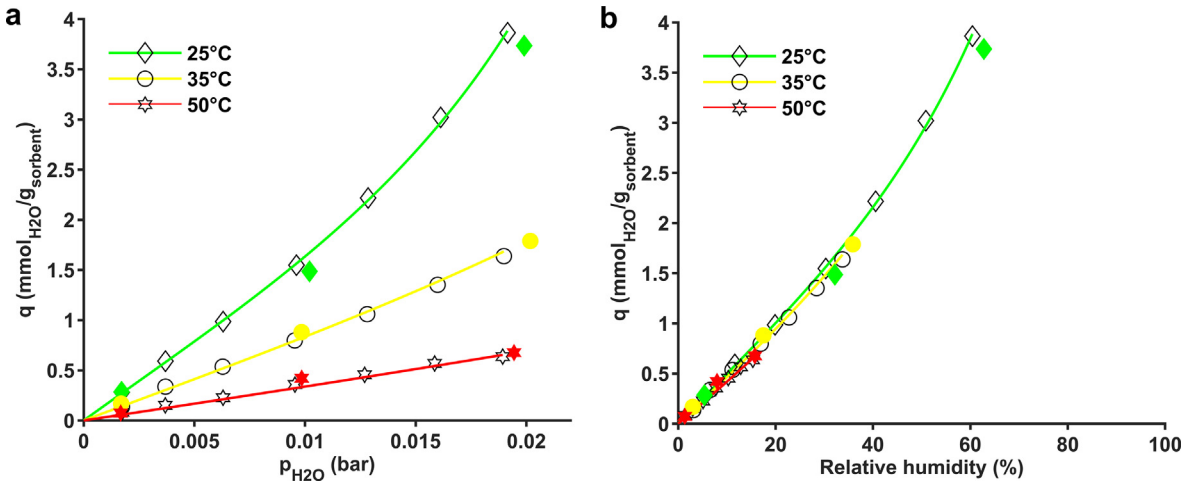

Fig. 2. Single-component H_2O desorption isotherms. Filled markers show H_2O desorption capacities in co-adsorption of 370–380 ppm CO_2 and humidity.

Table 2
Parameters of the GAB model fitted to single-component H_2O desorption isotherms, and the isosteric heat of H_2O adsorption at zero loading.

$q_{m,mono}$ (mmol$_{H2O}$/g$_{sorbent}$)	C_0	K_0	ΔH_C (kJ/mol	ΔH_K (kJ/mol)	$-\Delta H_{H2O,0}$
2.58	0.155	0.871	6.6	0	50.7

the single-component H_2O isotherm fits, and thus there is no need for a separate co-adsorption model in terms of H_2O adsorption in DAC conditions. Even with 4000 ppm CO_2, the resulting desorption capacities for H_2O were not significantly lower or higher than the single-component data, being 3.94 mmol$_{H2O}$/g$_{sorbent}$, 1.75 mmol$_{H2O}$/g$_{sorbent}$ and 0.75 mmol$_{H2O}$/g$_{sorbent}$ at 25 °C, 35 °C and 50 °C, respectively. The corresponding single-component points were 3.87 mmol$_{H2O}$/g$_{sorbent}$, 1.64 mmol$_{H2O}$/g$_{sorbent}$ and 0.64 mmol$_{H2O}$/g$_{sorbent}$. The results thus refer to CO_2 having a negligible effect on H_2O adsorption in terms of capacity at least with dilute CO_2. Similar behaviour was found for the amine-functionalized resin Lewatit VP OC 1065, even though H_2O is mostly adsorbed by the amine groups in amine-functionalized hydrophobic resins (Veneman et al., 2015). A possible reason for the unaffected H_2O capacity by CO_2 is that the groups that capture CO_2 also capture H_2O via the bicarbonate or hydronium carbamate formation as presented in Eqs. (3) and (4), respectively.

3.3. CO_2/H_2O co-adsorption isotherms

Even though the temperature-dependent Toth model has been used previously to model the CO_2 desorption isotherms of the aminoresin in both humid and dry conditions with excellent fits (Elfving et al., 2017; Elfving et al., 2017), the model lacks the effect of H_2O. Therefore, to model the CO_2 adsorption in variable temperature and humidity conditions, the model based on reaction kinetics of CO_2 and amines as presented in Eqs. (10)–(15) was used. As described in Section 2.2, the CO_2 adsorption rate equations were integrated to find the equilibrium capacities of CO_2, and the model was fitted to humid isotherm data of CO_2.

Fig. 3 shows the experimental humid CO_2 isotherms and the fit of the 5-parameter co-adsorption model of Eqs. (10)–(13). Overall, the 5-parameter model captures the temperature- and humidity dependency of the data well. The best fits to experimental data are obtained at 1 vol-% H_2O, with the modelled isotherms being very close to the experimental points. At 2 vol-%, some divergence from experimental data is shown especially in the low partial pressure region, with the model underestimating the capacity. At 25 °C, 19.9 mbar H_2O and 0.39 mbar CO_2, the experimental CO_2 capacity is 0.875 mmol$_{CO2}$/g$_{sorbent}$ and the model value is 0.827 mmol$_{CO2}$/g$_{sorbent}$. With 0.2 vol–% H_2O the isotherm fit diverges more from the experimental data especially at 25 °C by overestimating the capacity below 0.001 bar and underestimating it above this partial pressure. The experimental CO_2 capacity at 25 °C at 0.4 mbar CO_2 and 1.7 mbar H_2O is 0.572 mmol$_{CO2}$/g$_{sorbent}$ while the model estimate is 0.632 mmol$_{CO2}$/g$_{sorbent}$. Therefore, in DAC conditions at 25 °C, the model leads to a higher relative error of 10.5% at 0.2 vol-% H_2O vs. 5.5% at 2 vol-% H_2O.

To find whether the model fit to isotherm data could be improved, a 7-parameter model given by Eqs. (12)–(15) was used, where the exponents of the available amine site concentration are fitted parameters t_1 and t_2 instead of based on reaction stoichiometry as in the 5-parameter model. By letting the exponent parameters vary freely in the fitting procedure, it was expected that these parameters would increase, thus increasing the order of the model and explaining the data better. Fig. 4 shows the fit obtained with the 7-parameter co-adsorption model with relaxed boundaries of parameters t_1 and t_2. It is obvious that the model describes the experimental data excellently with the fitted exponential parameters of t_1 = 10.56 and t_2 = 14.42.

A variation of the 7-parameter model where the upper boundaries of the exponent parameters were set to 3 was also fitted to experimental data. This was done to limit the computational effort that could be expected to increase with high values of the exponential parameters. The fitted exponential parameters were found to be optimum at their upper limits, resulting in $t_1 = t_2 = 3$. Fig. S3 shows that while not yielding an almost perfect fit like the model with relaxed boundaries (Fig. 4), setting the upper boundaries of t_1 and t_2 to 3 resulted in a much better fit than with the 5-parameter model. Only at 25 °C with 0.2 vol-% H_2O at CO_2 partial pressures higher than 0.002 bar can the model be observed to significantly diverge from the experimental isotherm. Therefore, it seems that increased reaction order of the co-adsorption model also leads to a better fit of the isotherm data.

All the co-adsorption model-fit parameters are given in Table 3. Comparing the 5-parameter model maximum capacity of free

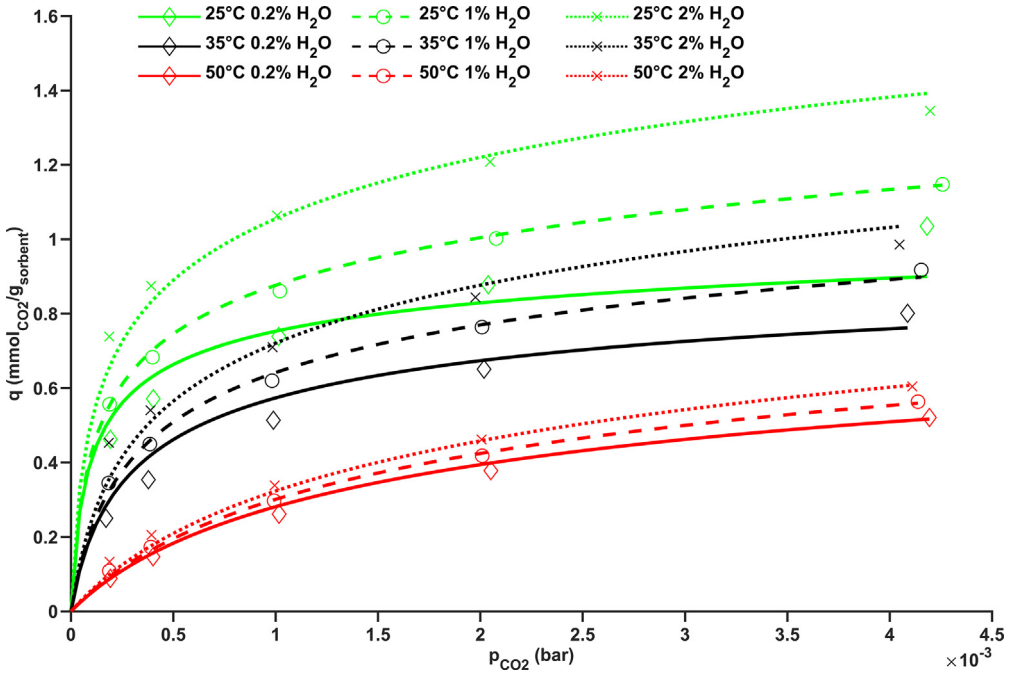

Fig. 3. Experimental (markers) and modelled (lines) CO_2 isotherms using the 5-parameter co-adsorption model.

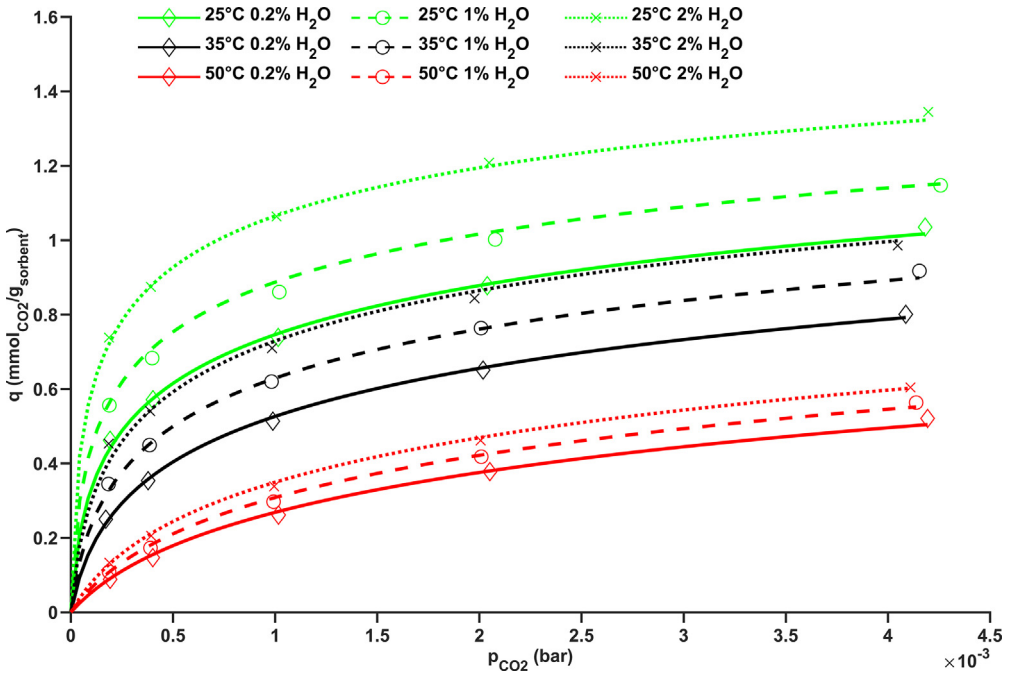

Fig. 4. Experimental (markers) and modelled (lines) CO_2 isotherms using the 7-parameter co-adsorption model with relaxed upper boundaries for parameters t_1 and t_2.

amine sites q_m of 1.91 $mmol_{amine}/g_{sorbent}$ to the amine content 4.72 $mmol_N/g_{sorbent}$ of the resin (Elfving et al., 2017) imparts that around 40% of the total amine capacity is available for CO_2. The 7-parameter model values for q_m are higher, and it is not deductible from the current data how accurately this parameter represents the value of free amine sites available for CO_2 capture. The isosteric heats of adsorption for the reactions in dry and humid conditions are 82–98 kJ/mol_{CO2} and 112–127 kJ/mol_{CO2}, respectively. The values for the humid reactions are higher, which is not expected if comparing the net reaction enthalpies of hydronium carbamate or bicarbonate and ammonium carbamate pathways (Li et al., 2016). However, (Miller et al., 2020) observed that while ammonium carbamate has a higher binding energy than hydronium carbamate, the hydrated form of hydronium carbamate has a binding energy higher than that of ammonium carbamate. Also, (Yu and Chuang, 2017) suggested the formation of hydrogen-bonded water/ammonium carbamate in humid CO_2 adsorption conditions on a TEPA film, which has a higher binding energy than ammonium carbamate. Comparing the values with literature, the isosteric heats of adsorption in reaction pathway 2 are somewhat high compared to other results for CO_2 capture on supported amines, such as 62–68 kJ/mol_{CO2} for the aminoresin in this study using the Toth

Table 3
Parameters of the kinetic co-adsorption models in isotherm data fitting.

Model	q_m ($mmol_{amine}/g_{sorbent}$)	$b_{0,1}$ ($bar^{-1}(mol/kg)^{1-t1}$)	$b_{0,2}$ ($bar^{-2}(mol/kg)^{1-t2}$)	t_1	t_2	$-\Delta H_1$ (kJ/mol)	$-\Delta H_2$ (kJ/mol)	$k_{f,1}$[a] ($bar^{-1}s^{-1}$ $(mol/kg)^{1-t1}$)	$k_{f,2}$[a] ($bar^{-2}s^{-1}\cdot(mol/kg)^{1-t2}$)
5-parameter	1.91	3.199E + 03	7.461E + 04	2	1	98.0	111.5	1	1
7-parameter	2.61	4.200E + 02	2.540E + 04	3[b]	3[b]	85.0	123.4	1	1
7-parameter	6.98	9.224E-06	7.372E-07	10.56	14.42	81.7	126.7	1	1

[a] Parameter value fixed.
[b] Parameter upper boundary fixed to 3.

model (Elfving et al., 2017), 87 kJ/mol_{CO2} for Lewatit VP OC 1065 (Veneman et al., 2015), 73 kJ/mol_{CO2} for NFC functionalized with aminosilane (Gebald, 2014) and around 90 kJ/mol_{CO2} for primary or secondary amine-containing SBA-15 (Alkhabbaz et al., 2014). The isosteric heats of adsorption from the co-adsorption models were used in the fixed-bed model heat balances to account for the adsorption heat of CO_2 from both ammonium carbamate and bicarbonate or hydronium carbamate formation.

It should be noted that the high values of t_1 and t_2 gained from the fitting of the 7-parameter model are probably not physically justified. It is known that amine-functionalized adsorbents are complex systems with multiple presented reaction pathways between CO_2, H_2O and amines as discussed in the introduction. In supported amine adsorbents, energetically different CO_2 adsorption sites can exist due to different amine groups and the hydrocarbon chains and groups linked to them (Alkhabbaz et al., 2014; Lee et al., 2018). However, there is no data on the current adsorbent to support the resulting high reaction orders of over 10. Especially, it can be deduced that in the case of the 7-parameter model, the resulting fitted t_1 and t_2 values do not represent the stoichiometry of the system. Therefore, the physicality of the exponent parameters in the case of the 7-parameter model fits is questionable, especially when no limits are set for these parameters.

The CO_2 capacity results gained from the lab-scale experiments and those given by the derived kinetic models exceed the results gained from pilot-scale experiments with the same adsorbent in real humid atmospheric conditions (Vidal Vázquez et al., 2018; Ruuskanen et al., 2021; Bajamundi et al., 2019). For example, during the DAC device performance campaigns the amount of adsorbed CO_2 varied between 0.5 and 0.7 $mmol_{CO2}/g_{sorbent}$, while temperature and relative humidity varied in the range of 15–20 °C and 39–78% (Bajamundi et al., 2019). However, the amount of pure CO_2 produced was only around 0.2–0.3 $mmol_{CO2}/g_{sorbent}$. This is due to incomplete regeneration of the resin in pilot-scale experiments using temperature-vacuum swing adsorption (TVSA) with desorption at around 80 °C. In dry laboratory-scale tests, this regeneration method (closed TVSA) was found to produce incomplete regeneration even at 100 °C (Elfving et al., 2021). In the pilot-scale experiments, TVSA was followed by a short temperature swing by flowing air through the hot beds leading to more desorbed but uncollected CO_2, which explains why the pilot-scale adsorption results are higher than the amounts produced. However, this TS-step was still not enough to completely regenerate the adsorbent due to low temperature, short desorption time and the presence of CO_2 in the feed. Therefore, to compare the capacities gained using the current model parameters to results gained in real ambient conditions with the same aminoresin, a more complete regeneration of the resin beds via use of, e.g., TVSA with steam stripping (Stampi-Bombelli et al., 2020; Sinha et al., 2017) or inert purge would be required.

3.4. Fixed-bed modelling of co-adsorption

To evaluate how well the kinetic co-adsorption model of CO_2 can be used to simulate adsorption column dynamics, the 5-parameter and 7-parameter co-adsorption models as well as the single-component H_2O GAB isotherm model were used in the source terms of the fixed-bed model described in Section 2.3. Here, the 7-parameter model with $t_1 = t_2 = 3$ was used in addition to the 5-parameter model in the fixed-bed data fitting.

Fig. 5 shows the results of the fixed-bed model fit to experimental data using the 5-parameter co-adsorption model. As seen in Fig. 5a, the CO_2 breakthrough profiles can be roughly divided into three regions: 1) the initial period of fast adsorption before and just after breakthrough with no increase or slow increase of CO_2 concentration; 2) a region of roughly linear concentration increase; 3) a region where adsorption slows down significantly, and the CO_2 concentration increases very slowly towards the feed concentration. The slowed-down kinetics may be due to CO_2 slowly reaching amine sites that are less easily accessed within the adsorbent pores, which become more hindered as more CO_2 is adsorbed. On the other hand, the resin has a fairly moderate amine loading of 4.7 $mmol_N/g_{sorbent}$ (Elfving et al., 2017) and adsorption of CO_2 on the aminoresin is clearly more equilibrium-controlled than diffusion-controlled such as in highly-loaded materials (Sayari et al., 2016; Goeppert et al., 2011). Another reason for the slowed-down kinetics than hindered amine sites may lie in the particle size distribution, with bigger particles taking longer to saturate than particles with a size close to the median of 0.6 mm (Elfving et al., 2017) or smaller.

Fig. 5a shows that at 25 °C in each humidity case, the model shows immediate breakthrough, while the experimental breakthrough times are between 10 and 13 min. After the initial period, the simulated CO_2 breakthrough curve at 0.2 vol-% H_2O shows a significantly delayed increase at around 23–60 min, while the other simulated curves follow the experimental data well. The result is expected due to the overestimation of the CO_2 adsorption capacity at 0.2 vol-% H_2O by the 5-parameter model (see Fig. 3). Also, in the last kinetic region, the simulated breakthrough curves in 0.2 vol-% and 2 vol-% H_2O cases reach the inlet concentration too early. However, at 1 vol-% H_2O, the model is also able to simulate the slowly increasing region with good accuracy, as shown in Fig. S4a.

Fig. 5b shows that the H_2O concentrations increase to near the inlet concentration in under 20 min, even at the lowest level of humidity. After one hour, there is very little change in the breakthrough profiles. It seems that the H_2O desorption isotherm coupled with the empty adsorption column model (see Fig. S2) underestimates the H_2O adsorption capacity at the lowest humidity content. Otherwise, the simulated H_2O breakthrough curves follow the experimental data well.

Fig. 5c shows that the magnitude of temperature increase is heavily dependent on the humidity content, and that this difference is well represented by the co-adsorption fixed-bed model. Experimental and simulated peak temperatures in the 2 vol-% case are around 35.5–35.7 °C, while in the 0.2 vol-% case, these are only around 26.5–27 °C. A 5–7 times higher temperature increase in the highest compared to lowest humidity content suggests that most of the released heat results from H_2O adsorption rather than CO_2 adsorption. After all, the CO_2 capacity is only around

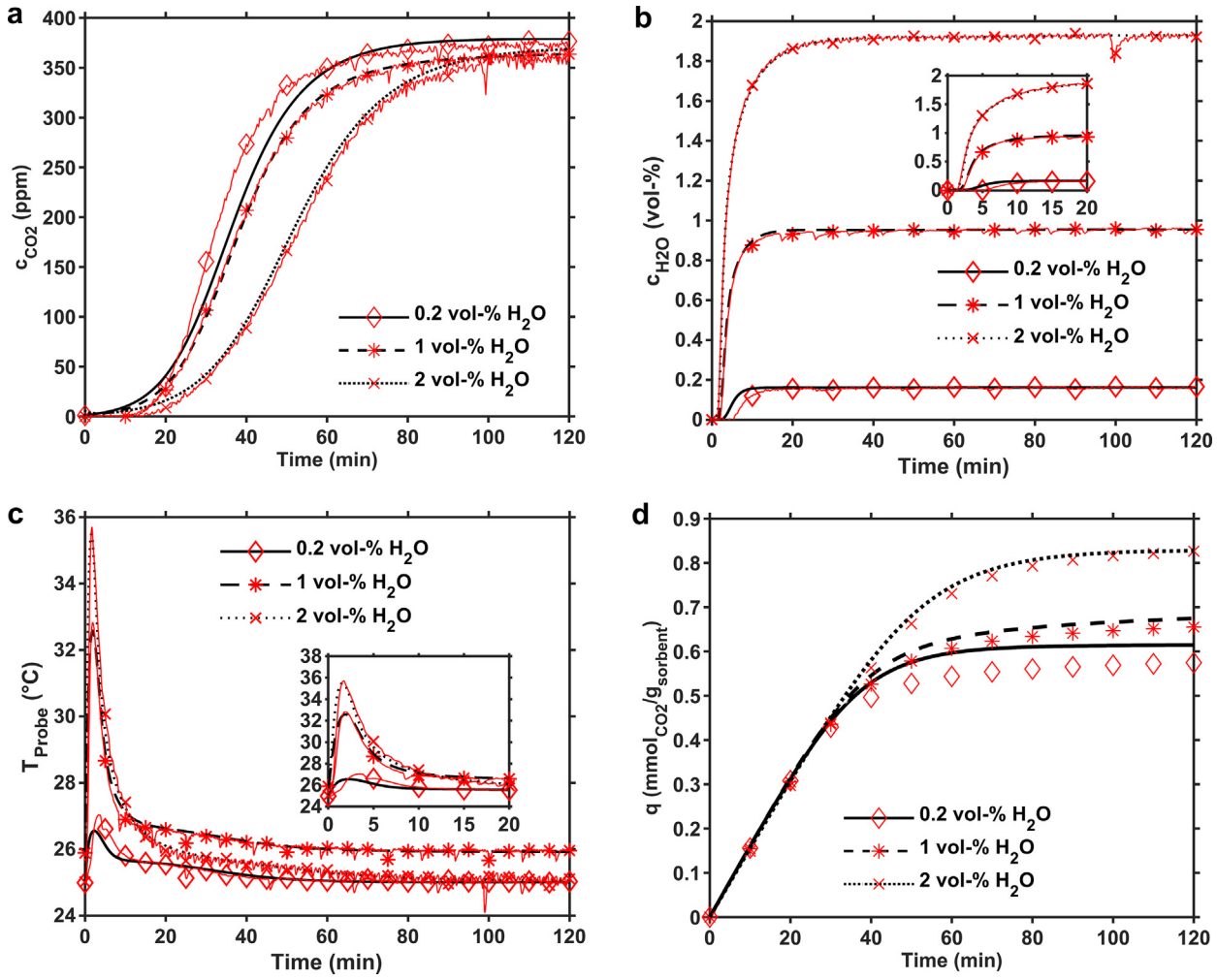

Fig. 5. Experimental (thin lines with markers) and simulated (lines) a) CO_2 breakthrough profiles; b) H_2O breakthrough profiles; c) bed temperature from probe 1 cm into the bed; d) CO_2 adsorption capacities from the first two hours of adsorption with initial bed temperature of 25 °C. For the 1 vol-% H_2O experiment, the initial bed temperature was 26 °C. The 5-parameter co-adsorption model was used to model CO_2 adsorption kinetics. The total flow rate was 500 ml/min. Inserts in b) and c) show the shape of the H_2O breakthrough curves and temperature from the first 20 min of the adsorption phase.

0.3 $mmol_{CO2}/_{sorbent}$ higher at 2 vol-% than at 0.2 vol-% H_2O, while the H_2O capacity is higher by over 3.5 $mmol_{CO2}/g_{sorbent}$. Also, as the heats of adsorption for the humid CO_2 adsorption reaction (Table 3) are comparable to the dry reaction heats of adsorption, the released heat per mole of adsorbed CO_2 is not significantly higher in humid vs. dry conditions. After the peak temperatures are reached, the decreasing temperature trends are also similar in simulated and experimental data. As the temperature changes are linked to the changes in H_2O concentration, the changes take place mostly in the first 20 min, therefore only affecting the initial region of CO_2 adsorption.

Fig. 5d shows that the dynamic CO_2 capacities appear similar until around 26–30 min, when the curves start to diverge. After this point, as expected from the CO_2 breakthrough profiles, the simulated CO_2 capacity curves of 0.2 vol-% and 2 vol-% cases reach their maximum values too early. In the 2 vol-% H_2O case, the simulated CO_2 capacity is around 0.83 $mmol_{CO2}/_{sorbent}$ at 120 min, after which practically no change is predicted. However, the experimental adsorption capacity continues to increase slowly up to 0.86 $mmol_{CO2}/_{sorbent}$ at five hours of adsorption. It should be taken into account that the experimental adsorption capacity curves were calculated via integration of the experimental breakthrough profiles, while the simulated capacity curves were calculated by co-adsorption models based on desorption capacities. Therefore, these capacity curves are never exactly the same.

Fig. 6a shows that at 35 °C, the simulated breakthrough curves follow the overall shape of the experimental curves closely for both 1 vol-% and 2 vol-% humidity cases. As in the 25 °C case, the model curves show immediate breakthrough, but the experimental breakthrough times are around 6–7 min. The initial kinetic region is better approximated by the model in the 2 vol-% case. However, the middle kinetic region is very closely followed by the model in both cases. In the region of slow adsorption rate (the upper part of the curve), the model slightly overestimates the concentration at first in both cases. However, the differences are only a few ppm or less.

Fig. 6b shows that the simulated H_2O breakthrough curves are again close to the experimental ones in the 1 and 2 vol-% H_2O cases. The breakthrough times are similar in simulated and experimental curves, all being close to 1 min. At around 6–30 min, a drop in H_2O concentration in the experimental data is visible, the reason for which is discussed in the Supplementary Data. As expected from the lower H_2O capacities at higher temperature and lower relative humidity, the temperature peaks are around 2–3 °C smaller than in the 25 °C case as shown in Fig. 6c. The experimental and simulated peak temperatures are around 40 °C at 1 vol-% H_2O and 42.5–43.5 °C at 2 vol-% H_2O.

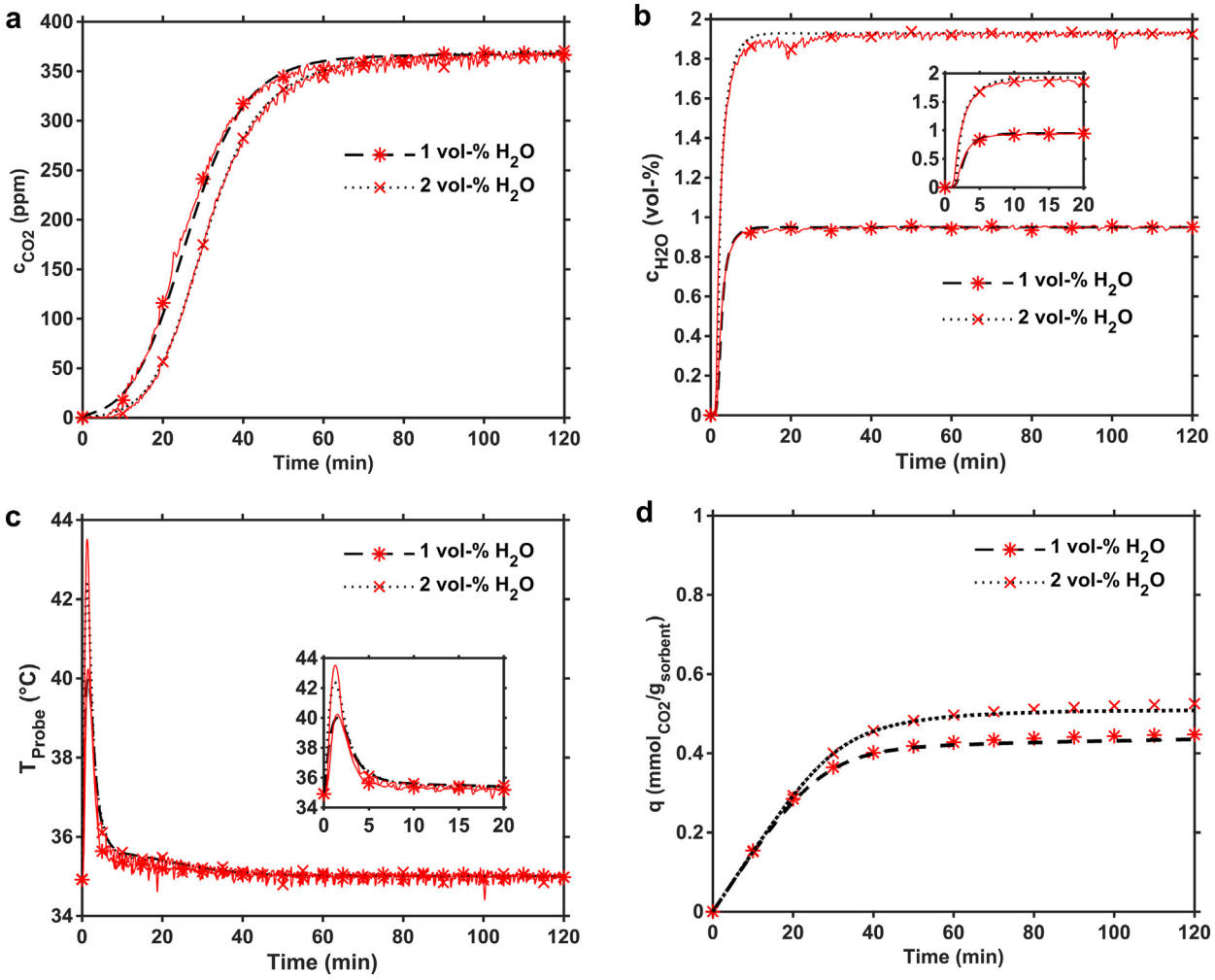

Fig. 6. Experimental (thin lines with markers) and simulated (lines) a) CO_2 breakthrough profiles; b) H_2O breakthrough profiles; c) bed temperature from probe 1 cm into the bed; d) CO_2 adsorption capacities from the first two hours of adsorption with initial bed temperature of 35 °C. The 5-parameter co-adsorption model was used to model CO_2 adsorption kinetics. The total flow rate was 500 ml/min. Inserts in b) and c) show the shape of the H_2O breakthrough curves and temperature from the first 20 min of the adsorption phase.

Fig. 6d shows that at 35 °C, the capacity profiles of 1 and 2 vol-% humidity cases start to diverge roughly 10 min from the start, with the model predictions following the experimental adsorption capacities closely for the first 120 min. However, similarly as to the case in a 25 °C setting, the model fails to predict the slowly increasing capacity trend after 120 min in the 2 vol-% H_2O case at 35 °C. However, in the 1 vol-% H_2O case, the modelled capacity increases gradually for the total duration of the experiment. The reason for these differences between humidity levels is apparent from the 5-parameter co-adsorption model fit (Fig. 3), where at each temperature the CO_2 capacity in DAC conditions (0.4 mbar CO_2) was best represented at 1 vol-% humidity.

To compare the adsorption rates, the experimental adsorption rates calculated from the first 30 min of adsorption are approximately 0.87 and 0.88 $mmol_{CO2}/(g_{sorbent}·h)$ at 1 and 2 vol-% H_2O at 25 °C, and 0.73 and 0.80 $mmol_{CO2}/(g_{sorbent}·h)$ at 1 and 2 vol-% H_2O at 35 °C, respectively. If calculated from the first 60 min of adsorption, the values are 0.61 and 0.73 $mmol_{CO2}/(g_{sorbent}·h)$ at 1 and 2 vol-% H_2O at 25 °C, and 0.43 and 0.50 $mmol_{CO2}/(g_{sorbent}·h)$ at 1 and 2 vol-% H_2O at 35 °C, respectively. Therefore, lower temperature and higher humidity content improve the CO_2 adsorption rate due to higher equilibrium adsorption capacity. Hahn et al., 2015 found that at levels of humidity content above 5 vol-%, the adsorption kinetics were retarded due to formation of water film around the adsorbent, thus limiting diffusion. Based on the results above, this might not be the case in DAC conditions, although studying CO_2 adsorption near 100% relative humidity is warranted.

Although the experimental dynamic adsorption data was mostly described well by the simulations using the 5-parameter model as discussed above, it is also clear that the shortcomings of the 5-parameter model in modelling of the CO_2 adsorption capacity translated into inaccuracies in the dynamic model. This can be deduced because the H_2O and temperature profiles were predicted well by the simulation and because the changes mostly took place before significant changes in CO_2 concentration started, as was shown above. Also, the worst CO_2 breakthrough simulations occurred when the CO_2 capacity was severely under- or overpredicted by the model. Thus, it could be expected that an improved co-adsorption model, that fits the isotherm data better than the 5-parameter model, should also yield a more accurate simulation of the adsorption process when used in the fixed-bed model. To this end, the 7–parameter co-adsorption model with $t_1 = t_2 = 3$ (Fig. S3) was used in the fixed-bed model.

Fig. 7 shows an overall better simulation of the CO_2 breakthrough with the 7-parameter model compared to using the 5-parameter model. Fig. 7a shows that the 7-parameter co-adsorption model improves the fit of the simulated CO_2 breakthrough curves, especially in the 0.2 vol-% H_2O case. At 0.2 vol-%

H_2O, the second kinetic region between 23 and 52 min is now closely represented by the model. In the slow adsorption region after 52 min, the model shows early saturation at 0.2 vol-%, but at 1 and 2 vol-% this region is also well represented by the model (also see Fig. S4). This is a clear improvement from using the 5-parameter co-adsorption model, which led to early saturation at 2 vol-% humidity. This is also seen in the capacity curves in Fig. 7b, where capacity in the 2 vol-% case keeps increasing after 120 min. Compared to the 5-parameter model results at 2 vol-% H_2O and 25 °C, where practically no change was observed after two hours, the simulated capacity here still increases from around 0.86 $mmol_{CO2}/g_{sorbent}$ at two hours to almost 0.88 $mmol_{CO2}/g_{sorbent}$ at five hours.

To find the effect of flow rate on the CO_2 adsorption process, a nearly 2-day adsorption from humidified compressed air was done using a low flow rate (100 ml/min). Fig. 8 shows the experimental and simulated results of this run using the 5-parameter and 7-parameter (t_1 = t_2 = 3) kinetic models in the fixed-bed model. As shown in Fig. 8a, the CO_2 breakthrough ($c_{CO2}/c_{CO2,feed}$ > 0.01) is well predicted by both models, and occurs at 192–194 min in the experiment and at around 180–190 min in the simulations. In the second kinetic region using the 7-parameter model, a significant divergence of the simulated breakthrough curve from the experimental curve is seen after around 230 min. On the other hand, both simulated curves reach saturation too early, being at 401 ppm after around 14 h of adsorption, while the experimental concentration is around 395 ppm at this point.

By the time CO_2 breakthrough occurs, the experimental H_2O profile is almost at the inlet H_2O concentration as shown in Fig. 8b. Overall, the simulated H_2O curve represents the experimental profile well, although the feed concentration is reached somewhat early. The differences between the simulated and experimental H_2O breakthrough curves are only a few hundred ppm at highest, and their effect on CO_2 adsorption dynamics can be assumed negligible. The magnitude of temperature increase is captured well by the simulations as shown in Fig. 8c, where both the experimental and simulated probe temperatures reach a peak of around 28.5 °C. The figure also shows an interesting shape of the temperature profile not clearly seen in the 500 ml/min experiments. At around 80–280 min, a shoulder appears with a temperature of 25.1–25.2 °C before cooling down to 24.9 °C. The cause of this shoulder is evident when comparing it with the CO_2 breakthrough data, imparting that this delay in cooling is caused by the heat released from the adsorption of CO_2.

The difference between the experimental and simulated adsorption capacities in the 2-day run can be seen from Fig. 8d. It is clear that both models underpredict the experimental pseudo-equilibrium capacity of 0.92 $mmol_{CO2}/g_{sorbent}$, which is probably the main reason why the simulated CO_2 breakthrough profiles represented the slow kinetic region poorly. However, it is notable here that although the 7-parameter co-adsorption model gives a closer estimation of the pseudo-equilibrium CO_2 capacity, the breakthrough curves fitted using this model are worse than by using the 5-parameter model. This is contrary to the results found for the 500 ml/min cases, and imparts that the 7-parameter model does not necessarily give a better estimation of the adsorption kinetics, although the isotherm fit is significantly improved compared to the 5-parameter model. On the other hand, in the case of the 7-parameter model, the selection of the upper boundary for the exponential parameters during isotherm fitting was arbitrary, and it should be assessed in more detail how these affect the performance of the model in different hydrodynamic conditions. However, as flow rate affects the mass transfer resistances in CO_2 adsorption, the reason for the worse performance of both models in the low flow rate case may in part be caused by the lack of separate diffusional models for CO_2. This will be discussed in more detail later in the text.

In terms of the CO_2 breakthrough curve shape and challenges in simulating the slow approach to feed concentration encountered with each of the models, similar observations have been reported in the literature. Bollini et al. (2012) found the LDF kinetic model combined with the Toth isotherm insufficient to describe CO_2 adsorption kinetics on adsorbents with high amine loadings. Better results were obtained by using a heterogeneous model that takes into account two diffusion mechanisms in the adsorbent: fast diffusion in the pores and slow diffusion in the aminopolymer phase. However, even with this heterogeneous model their results showed premature saturation, failing to represent the upper part of the CO_2 breakthrough curve. Serna-Guerrero and Sayari (2010) used the Toth isotherm model and Avrami kinetic model for CO_2 adsorption in dry flue-gas conditions on amine-grafted silica. Their simulation also shows an excessively fast approach of saturation in some experiments, although they attributed this to experimental error rather than actual kinetic behaviour. Jung and Lee (2020) used a reaction mechanism-based kinetic model such as in this work to simulate the CO_2 adsorption breakthrough curves in humid flue gas conditions on PEI-functionalized silica. Also in their

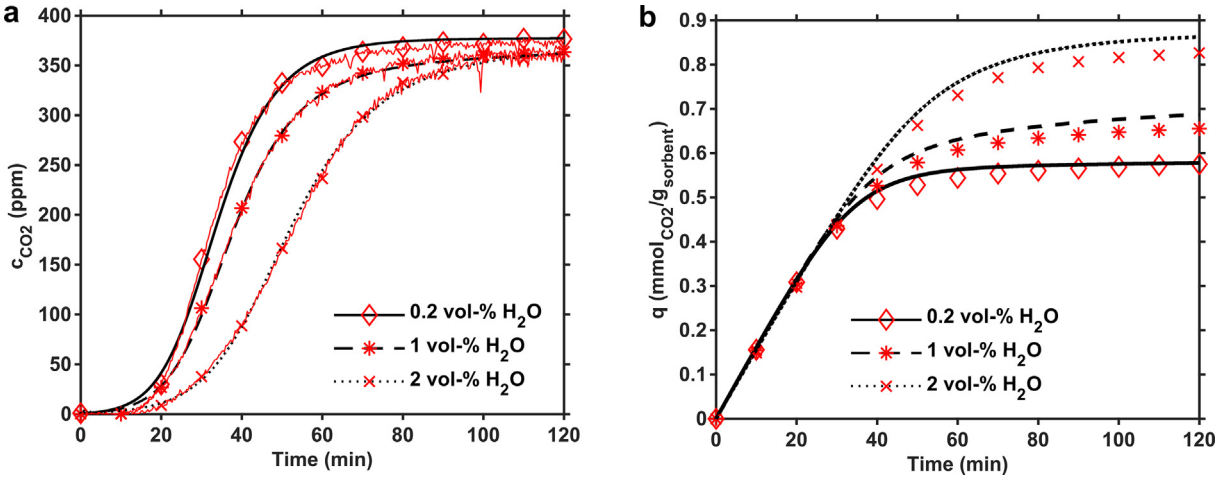

Fig. 7. Experimental (thin lines with markers) and simulated (lines) a) CO_2 breakthrough profiles; b) CO_2 adsorption capacities from the first two hours of adsorption. The 7-parameter co-adsorption model with t_1 = t_2 = 3 was used to model CO_2 adsorption kinetics. The total flow rate was 500 ml/min. Initial bed temperature was 25 °C, except for 1 vol-% H_2O experiment where it was 26 °C.

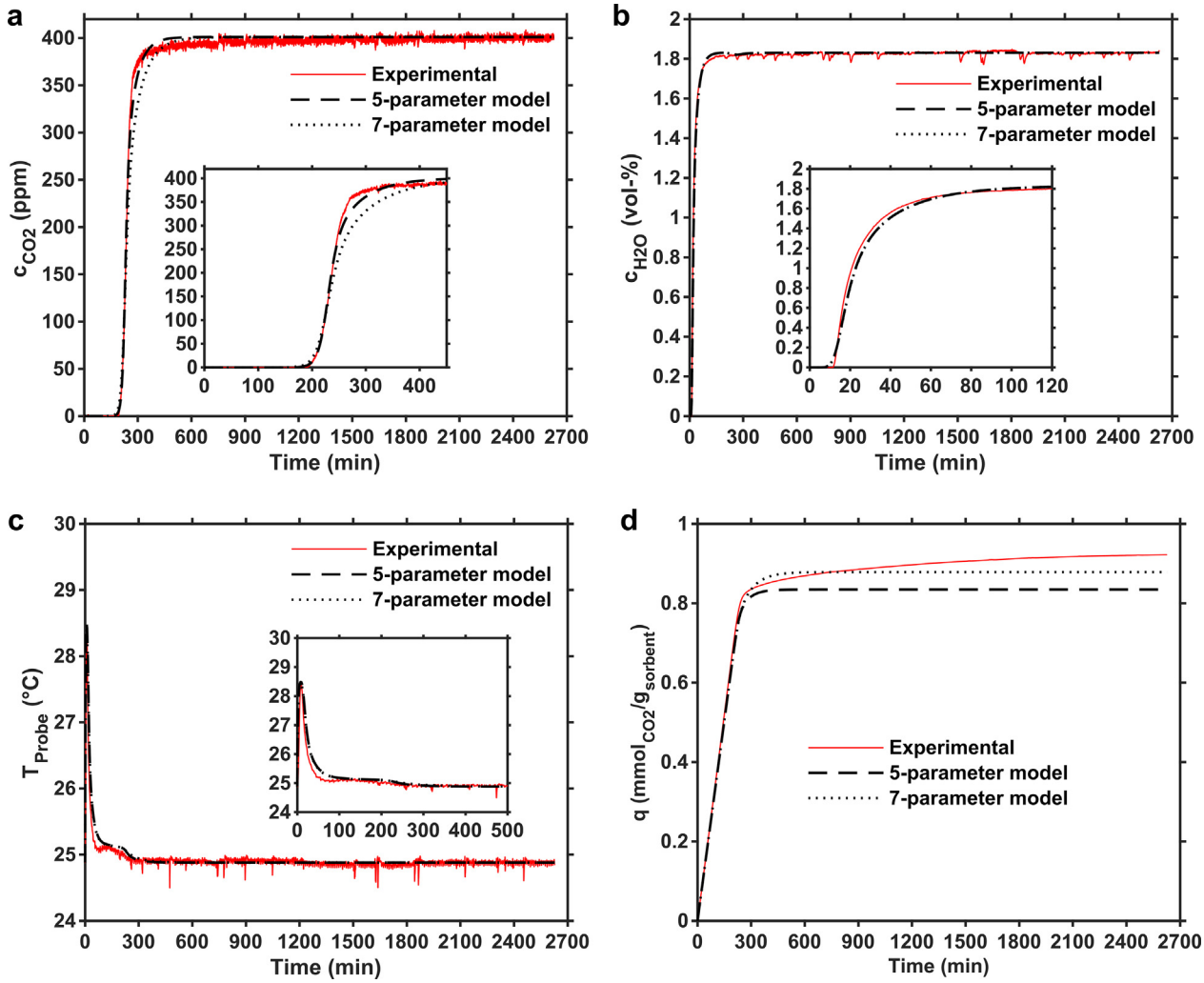

Fig. 8. Experimental (thin lines with markers) and simulated (lines) a) CO_2 breakthrough profiles; b) H_2O breakthrough profiles; c) bed temperature from probe 1 cm into the bed; d) CO_2 adsorption capacities with a flow rate of 100 ml/min and initial bed temperature of 25 °C. In the 7-parameter co-adsorption model $t_1 = t_2 = 3$.

work, the simulations often seemed to show early increase of the CO_2 concentration to feed conditions compared to experimental data, although the difference did not seem pronounced.

Since the concentration of adsorbate affects the velocity of the concentration fronts and the shape of the breakthrough curves, the best reference data for this study would be acquired under DAC conditions. Even though DAC on supported amine adsorbents has been simulated in several studies (Wurzbacher et al., 2016; Stampi-Bombelli et al., 2020; Sinha et al., 2017; Darunte et al., 2019), comparisons of fixed-bed models to experimental data are rare, especially under humid conditions. Darunte et al. (2019) reported the modelling of CO_2 adsorption on diamine-functionalized Mg_2(dobpdc) MOF adsorbent, which had an interesting isotherm shape requiring splitting of both the isotherm model and the kinetic regions into two parts. By combining LDF and Avrami models, they simulated the CO_2 breakthrough profiles in dry DAC conditions, exhibiting a comparison to experimental data. However, due to the peculiar shape of the CO_2 isotherms and breakthrough curves, their results are difficult to compare with those observed with typical type-1 or Langmuir-shape isotherms. Stampi-Bombelli et al. (2020) found somewhat good representation by their fixed-bed model prediction of the CO_2 adsorption breakthrough curve in humid DAC conditions using the modified Toth isotherm and the LDF kinetic model. However, due to use of a very flat-shaped adsorbent bed with a height-to-width ratio of 1/8, the shape of the breakthrough curve was very different from those reported in this work, making it difficult to make any comparisons of the kinetics.

The CO_2 adsorption simulations in DAC (Wurzbacher et al., 2016; Stampi-Bombelli et al., 2020; Sinha et al., 2017; Darunte et al., 2019) or PCC conditions (Bollini et al., 2012; Shafeeyan et al., 2014; Haghpanah et al., 2013) typically rely on the use of separate isotherm and kinetic models. Although the most important aspect of the current kinetic approach is the ability to model the effect of humidity on CO_2 adsorption, this approach may also lead to other advantages over the conventional approach with separate isotherm and kinetic models. To study these differences, a comparison was made between the Toth isotherm coupled with the LDF kinetic model and the kinetic approach of the current work, which can be found in the Supplementary Data. Fig. S6 shows that while the differences are fairly small, the 5-parameter and 7-parameter models give a better prediction of the overall shape of the CO_2 breakthrough curve, especially when the model capacity prediction matches the experimental one. Additionally, the 5-parameter and 7-parameter models have comparable computational times with the Toth + LDF model. While higher-order kinetic models such as the Avrami model may give a better representation of the breakthrough curve than the LDF model, they can

be expected to lead to higher computational effort. Further, given that more complex isotherm models are required to take humidity into account like the 5/7-parameter models do, thus further increasing the computational cost, the kinetic approach presented in the current work also seems numerically more advantageous compared to using separate models for equilibrium and kinetics. In the conventional approach, an improved kinetic model such as the Avrami model, and an isotherm model taking humidity into account, also come with additional uncertainty related to the additional parameters required.

The best-fit parameters of the fixed-bed model are given in Table 4. The kinetic parameter $k_{f,2}$ increases compared to $k_{f,1}$ with humidity, which could result from shift to bicarbonate or hydronium carbamate formation as humidity content increases. Additionally, the $k_{f,2}$ parameter is lower at 35 °C at both 1 and 2 vol-% H_2O. The decreased value of the $k_{f,2}$ parameter is probably related to retarded adsorption reaction kinetics rather than mass transfer, since higher temperature should increase mass transfer. This is observed in the case of the Toth + LDF model fit, where the LDF kinetic parameter is higher at 35 °C compared to 25 °C. However, it should be taken into account that the kinetic parameters for the three models are apparent rather than intrinsic, combining all the mass transfer resistances as well as CO_2 adsorption reaction kinetics.

The $k_{f,1}$ and $k_{f,2}$ values in the 500 ml/min case are not identical to those in the 100 ml/min case at 25 °C, while these should be constant with flow rate if the parameters only described adsorption reaction kinetics and intraparticle diffusion. While intraparticle diffusion and the adsorption reaction kinetics are not affected by hydrodynamic conditions such as flow rate (Ruthven, 1984), the external fluid film resistance can be expected to be much higher in the 100 ml/min experiment compared to the 500 ml/min experiments. Therefore, the results impart that external fluid film resistance around the adsorbent particle has a significant effect on the kinetics at least in the studied conditions. Therefore, in addition to the proposed co-adsorption models, a more accurate and generalized treatment of the adsorption kinetics requires additional models that take into account the diffusion of CO_2 in the adsorbent particle. This includes diffusion through the external film of the particle and intraparticle diffusion. Of these, the film mass transfer is probably more important, but it should also be assessed if diffusional resistances inside the particle can be neglected or not, such as in Bos et al. (Bos et al., 2019).

Other limitations related to the models and the experimental device also existed, which should be taken into account when comparing the parameters in Table 4. The adsorption column only had one temperature probe, and therefore it was not possible to record axial distribution of temperature, which could affect the adsorption rate in the fixed-bed. The estimated value of the K_z parameter was typically near its initial value, which was 2 W/(m·K) in all of the data fittings. To find the true temperature distribution and its effect on the adsorption process, experimental data would be required from several points along the column in the axial direction. Moreover, the way that the effect of the empty volume on the H_2O material balance is taken into account (see Section 2.3) increases the released heat, affecting the overall heat transfer coefficients represented by h. In this work, only the adsorbent bed was simulated, but in future work, a detailed model of the dead volume in the experimental device should be included. Also, in the 100 ml/min case, both kinetic models yielded lower CO_2 adsorption capacities than determined experimentally, which also had an effect on the dynamic model fit and thus the kinetic parameters.

The overall shape of CO_2 adsorption breakthrough curves was simulated well by the 5/7-parameter models used in this work. When the pseudo-equilibrium isotherm points were close to the model values, even the upper part of the breakthrough curve was closely represented. However, when using a low flow rate of 100 ml/min leading to extended adsorption time, difficulties arose in reproducing the shape of the entire breakthrough curve. The co-adsorption model equilibrium parameters were obtained by fitting to pseudo-equilibrium isotherms rather than true equilibrium data. The kinetic parameters of the co-adsorption models, $k_{f,1}$ and $k_{f,2}$, were obtained by fitting the dynamic model to CO_2 breakthrough data, without separately taking into account diffusional

Table 4
Parameters of the fixed-bed model fits at different temperatures, humidities and flow rates. The axial dispersion coefficient was calculated by using a correlation, while all the other listed parameters were fitted.

Case and CO_2 adsorption model	D_L (m^2/s)	$k_{f,1}$ ($bar^{-1}s^{-1}\cdot(mol/kg)^{1-t1}$)[a]	$k_{f,2}$ ($bar^{-2}s^{-1}\cdot(mol/kg)^{1-t2}$)	$k_{H2O,LDF}$ (1/s)	K_z ($Wm^{-1}K^{-1}$)	h ($Wm^{-2}K^{-1}$)
0.2 vol-% H_2O 25 °C 5 parameter model	3.50E-04	1.37	1.71	0.99	1.74	17.78
1 vol-% H_2O 26 °C 5 parameter model	3.50E-04	1.48	12.67	0.38	2.12	10.51
2 vol-% H_2O 25 °C 5 parameter model	3.50E-04	0.92	58.74	0.22	2.10	17.34
1 vol-% H_2O 35 °C 5 parameter model	3.52E-04	1.35	2.06	0.26	1.96	19.65
2 vol-% H_2O 35 °C 5 parameter model	3.51E-04	1.78	14.54	0.88	1.96	36.25
0.2 vol-% H_2O 25 °C 7 parameter model ($t_1 = t_2 = 3$)	3.50E-04	0.35	2.33	1.22	1.96	11.87
1 vol-% H_2O 26 °C 7 parameter model ($t_1 = t_2 = 3$)	3.50E-04	0.32	4.94	0.39	2.0	10.13
2 vol-% H_2O 25 °C 7 parameter model ($t_1 = t_2 = 3$)	3.50E-04	0.20	8.53	0.20	2.10	18.90
2 vol-% H_2O 35 °C 7 parameter model ($t_1 = t_2 = 3$)	3.51E-04	0.45	3.57	1.60	3.12	33.12
2 vol-% H_2O 25 °C, 100 ml/min 5 parameter model	7.44E-05	3.81	30.25	0.11	2.03	18.13
2 vol-% H_2O 25 °C, 100 ml/min 7 parameter model ($t_1 = t_2 = 3$)	7.44E-05	0.69	5.03	0.10	2.10	18.59
2 vol-% H_2O 25 °C Toth + LDF	3.50E-04	0.0012 s^{-1}	–	0.29	1.86	16.67
2 vol-% H_2O 35 °C Toth + LDF	3.51E-04	0.0018 s^{-1}	–	0.20	1.89	30.13

[a] For Toth + LDF, the LDF kinetic constant reported.

resistances in the adsorbent particle. Therefore, perfect simulation of the breakthrough curves for very long adsorption runs would probably require true equilibrium isotherms determined from adsorption capacities measured for several days, and possibly a separate model of CO_2 diffusion in the adsorbent. On the other hand, one may argue that adsorption steps lasting several days instead of several hours would not be economically viable, as an optimized DAC process is most likely operated with much shorter cycles. Therefore, the strong representation of the experimental fixed-bed data in this work already warrants the use of these co-adsorption models in simulation of humid DAC to study the dynamics of CO_2 adsorption and the related specific energy requirement.

4. Conclusions

In this work, CO_2 adsorption from air was simulated by using a kinetic model which takes into account the effect of humidity, the study of which has been all but neglected in scientific literature so far. Pseudo-equilibrium CO_2 isotherms in humid conditions with partial pressures of CO_2 and H_2O relevant to DAC were measured experimentally at 25–50 °C on an amine-functionalized resin. The kinetic co-adsorption model based on reaction mechanisms of CO_2 with amines in dry and humid conditions was used to calculate the equilibrium CO_2 capacities and fitted to the experimental isotherm data. To account for the adsorption of humidity, the temperature-dependent GAB model was fitted to experimental single-component H_2O isotherms. The co-adsorption model accounting for CO_2 adsorption kinetics and the GAB model coupled with the linear driving force model describing H_2O adsorption kinetics were then used in a dynamic non-isothermal model. This model was fitted against experimental CO_2 and H_2O breakthrough curves and adsorption column temperature in DAC conditions. A humid cyclic adsorption/desorption experiment was also done to find the capacity drop rate.

In the cyclic experiment, a CO_2 capacity drop of approximately 0.7%/cycle was measured, which necessitated the correction of experimental isotherm data to account for the drop in capacity. The H_2O isotherms were well approximated by the GAB isotherm with multilayer H_2O adsorption behavior. In all studied CO_2 partial pressures and temperatures, increased humidity content led to an increase in CO_2 capacity. This phenomenon was captured well by the proposed kinetic co-adsorption model, of which three variations with different reaction orders were used. The 5-parameter model with reaction order based on reaction stoichiometry gave an overall good fit to the isotherms, but at the lowest humidity content of 0.2 vol-% led to overprediction of the CO_2 capacity at partial pressures lower than 0.001 bar. The so-called 7-parameter model with a higher but arbitrary reaction order yielded an almost perfect fit to the isotherm data. In fitting the fixed-bed model to dynamic experimental data, the simulated breakthrough curves and adsorption column temperature were close to the experimental ones. It was found that the accuracy of the CO_2 isotherm fit given by the kinetic co-adsorption model significantly affected the accuracy of the simulated CO_2 breakthrough curves. Using the 7-parameter kinetic model in the dynamic model also yielded close representation of the whole CO_2 breakthrough profile in cases where the 5-parameter model failed.

The present work used pseudo-equilibrium CO_2 isotherm data from several-hour experiments and used the co-adsorption models directly to model the kinetics of CO_2 adsorption without separately accounting for the effect of diffusional resistances in the adsorbent particle. Possibly due to these reasons, at a lower flow rate of 100 ml/min, the fixed-bed model fit represented the CO_2 breakthrough time well but failed to simulate the long, slowly increasing upper part of the concentration profile. Therefore, for determining mass-transfer parameters valid for scale-up, the effect of diffusional resistances in the adsorbent particle should be assessed in future studies. To realistically account for heat transfer in different bed shapes, 2-D simulation coupled with temperature measurement from several points in axial and radial directions should be used. To include desorption, the current parameters of the co-adsorption kinetic models may be used as a first estimate, but for more accurate simulation of CO_2 production, adsorption capacities measured at higher partial pressures of CO_2 should also be included in the isotherm fitting.

Nevertheless, even in the current form, 1-D fixed-bed adsorption simulation with the proposed co-adsorption kinetic models help assess critical parameters of CO_2 adsorption in humid DAC conditions such as adsorption rate and specific energy requirement in different conditions. Moreover, based on a preliminary comparison, using the proposed models to simulate CO_2 adsorption kinetics instead of separate isotherm and kinetic models can yield both improved accuracy and numerical advantage. For purposes of scaling up, the proposed kinetic models can be combined with existing mass-transfer models. Thus, the presented co-adsorption models are expected to be generally useful in the modelling of CO_2 adsorption kinetics on amine-functionalized adsorbents.

CRediT authorship contribution statement

Jere Elfving: Conceptualization, Methodology, Software, Validation, Formal analysis, Investigation, Data curation, Writing - original draft, Writing - review & editing, Visualization, Project administration, Funding acquisition. **Tuomo Sainio:** Methodology, Writing - review & editing, Supervision.

Declaration of Competing Interest

The authors declare that they have no known competing financial interests or personal relationships that could have appeared to influence the work reported in this paper.

Acknowledgements

This study was conducted as a part of the DAC2.0 project funded by the Academy of Finland under grant number 329312.

The authors would also like to thank Dr. Harri Nieminen for his useful comments on the manuscript.

Appendix A. Supplementary material

Supplementary data to this article can be found online at https://doi.org/10.1016/j.ces.2021.116885.

References

Coninck, H., Revi, A., Babiker, M., Bertoldi, P., Buckeridge, M., Cartwright, A., Dong, W., Ford, J., Fuss, S., Hourcade, J.-C., Ley, D., Mechler, R., Newman, P., Revokatova, A., Schultz, S., Steg, L., Sugiyama, T., 2018. IPCC special report - Global warming of 1.5 °C: Chapter 4 - Strengthening and implementing the global response. https://www.ipcc.ch/site/assets/uploads/sites/2/2019/05/SR15_Chapter4_Low_Res.pdf.

Sanz-Pérez, E.S., Murdock, C.R., Didas, S.A., Jones, C.W., 2016. Direct capture of CO_2 from ambient air. Chem. Rev. 116, 11840–11876. https://doi.org/10.1021/acs.chemrev.6b00173.

de Jonge, M.M.J., Daemen, J., Loriaux, J.M., Steinmann, Z.J.N., Huijbregts, M.A.J., 2019. Life cycle carbon efficiency of direct air capture systems with strong hydroxide sorbents. Int. J. Greenh. Gas Control. 80, 25–31. https://doi.org/10.1016/j.ijggc.2018.11.011.

Deutz, S., Bardow, A., 2021. Life-cycle assessment of an industrial direct air capture process based on temperature–vacuum swing adsorption. Nat. Energy. 6, 203–213. https://doi.org/10.1038/s41560-020-00771-9.

Breyer, C., Fasihi, M., Bajamundi, C., Creutzig, F., 2019. Direct air capture of CO_2: A key technology for ambitious climate change mitigation. Joule. 3, 2053–2057. https://doi.org/10.1016/j.joule.2019.08.010.

Fuss, S., Lamb, W.F., Callaghan, M.W., Hilaire, J., Creutzig, F., Amann, T., Beringer, T., De Oliveira Garcia, W., Hartmann, J., Khanna, T., Luderer, G., Nemet, G.F., Rogelj, J., Smith, P., Vicente, J.L.V., Wilcox, J., Del Mar Zamora Dominguez, M., Minx, J.C., 2018. Negative emissions - Part 2: Costs, potentials and side effects. Environ. Res. Lett. 13,. https://doi.org/10.1088/1748-9326/aabf9f 063002.

Vidal Vázquez, F., Koponen, J., Ruuskanen, V., Bajamundi, C., Kosonen, A., Simell, P., Ahola, J., Frilund, C., Elfving, J., Reinikainen, M., Heikkinen, N., Kauppinen, J., Piermartini, P., 2018. Power-to-X technology using renewable electricity and carbon dioxide from ambient air: SOLETAIR proof-of-concept and improved process concept. J. CO_2 Util. 28, 235–246. https://doi.org/10.1016/j.jcou.2018.09.026.

Rodríguez-Mosqueda, R., Rutgers, J., Bramer, E.A., Brem, G., 2019. Low temperature water vapor pressure swing for the regeneration of adsorbents for CO_2 enrichment in greenhouses via direct air capture. J. CO2 Util. 29, 65–73. https://doi.org/10.1016/j.jcou.2018.11.010.

Ruuskanen, V., Givirovskiy, G., Elfving, J., Kokkonen, P., Karvinen, A., Järvinen, L., Sillman, J., Vainikka, M., Ahola, J., 2021. Neo-Carbon Food concept: A pilot-scale hybrid biological–inorganic system with direct air capture of carbon dioxide. J. Clean. Prod. 278,. https://doi.org/10.1016/j.jclepro.2020.123423 123423.

Keith, D.W., Holmes, G., St Angelo, D., Heidel, K., 2018. A process for capturing CO_2 from the atmosphere. Joule 2, 1573–1594. https://doi.org/10.1016/j.joule.2018.05.006.

Fasihi, M., Efimova, O., Breyer, C., 2019. Techno-economic assessment of CO_2 direct air capture plants. J. Clean. Prod. 224, 957–980. https://doi.org/10.1016/j.jclepro.2019.03.086.

Shi, X., Li, Q., Wang, T., Lackner, K.S., 2017. Kinetic analysis of an anion exchange absorbent for CO2 capture from ambient air. PLoS One. 12, 1–12. https://doi.org/10.1371/journal.pone.0179828.

Van Der Giesen, C., Meinrenken, C.J., Kleijn, R., Sprecher, B., Lackner, K.S., Kramer, G. J., 2017. A life-cycle assessment case study of coal-fired electricity generation with humidity swing direct air capture of CO_2 versus mea-based postcombustion capture. Environ. Sci. Technol. 51, 1024–1034. https://doi.org/10.1021/acs.est.6b05028.

Bajamundi, C.J.E., Koponen, J., Ruuskanen, V., Elfving, J., Kosonen, A., Kauppinen, J., Ahola, J., 2019. Capturing CO_2 from air: Technical performance and process control improvement. J. CO2 Util. 30, 232–239. https://doi.org/10.1016/j.jcou.2019.02.002.

Wurzbacher, J.A., Gebald, C., Brunner, S., Steinfeld, A., 2016. Heat and mass transfer of temperature-vacuum swing desorption for CO_2 capture from air. Chem. Eng. J. 283, 1329–1338. https://doi.org/10.1016/j.cej.2015.08.035.

Climeworks, subsite: "CO2 removal," (2021). https://www.climeworks.com (accessed June 10, 2021).

Shi, X., Xiao, H., Azarabadi, H., Song, J., Wu, X., Chen, X., Lackner, K.S., 2020. Sorbents for the direct capture of CO_2 from ambient air. Angew. Chemie - Int. Ed. 59, 6984–7006. https://doi.org/10.1002/anie.201906756.

Drechsler, C., Agar, D.W., 2020. Investigation of water co-adsorption on the energy balance of solid sorbent based direct air capture processes. Energy. 192,. https://doi.org/10.1016/j.energy.2019.116587 116587.

Veneman, R., Natalia, F., Wenying, Z., Zhenshan, L., Sascha, K., Brilman, W., 2015. Adsorption of H_2O and CO_2 on supported amine sorbents. Int. J. Greenh. Gas Control. 41, 268–275. https://doi.org/http://dx.doi.org/10.1016/j.ijggc.2015.07.014.

Gebald, C., Wurzbacher, J.A., Borgschulte, A., Zimmermann, T., Steinfeld, A., 2014. Single-component and binary CO2 and H2O adsorption of amine-functionalized cellulose. Environ. Sci. Technol. 48, 2497–2504. https://doi.org/10.1021/es404430g.

Jahandar Lashaki, M., Khiavi, S., Sayari, A., 2019. Stability of amine-functionalized CO_2 adsorbents: A multifaceted puzzle. Chem. Soc. Rev. 48, 3320–3405. https://doi.org/10.1039/c8cs00877a.

Choi, S., Drese, J.H., Jones, C.W., 2009. Adsorbent materials for carbon dioxide capture from large anthropogenic point sources. ChemSusChem 2, 796–854. https://doi.org/10.1002/cssc.200900036.

Li, K., Kress, J.D., Mebane, D.S., 2016. The mechanism of CO_2 adsorption under dry and humid conditions in mesoporous silica-supported amine sorbents. J. Phys. Chem. C 120, 23683–23691. https://doi.org/10.1021/acs.jpcc.6b08808.

Lee, J.J., Chen, C.H., Shimon, D., Hayes, S.E., Sievers, C., Jones, C.W., 2017. Effect of humidity on the CO_2 adsorption of tertiary amine grafted SBA-15. J. Phys. Chem. C 121, 23480–23487. https://doi.org/10.1021/acs.jpcc.7b07930.

Didas, S.A., Sakwa-Novak, M.A., Foo, G.S., Sievers, C., Jones, C.W., 2014. Effect of amine surface coverage on the co-adsorption of CO2 and water: spectral deconvolution of adsorbed species. J. Phys. Chem. Lett. 5, 4194–4200. https://doi.org/10.1021/jz502032c.

Chen, C.H., Shimon, D., Lee, J.J., Mentink-Vigier, F., Hung, I., Sievers, C., Jones, C.W., Hayes, S.E., 2018. The "missing" bicarbonate in CO_2 chemisorption reactions on solid amine sorbents. J. Am. Chem. Soc. 140, 8648–8651. https://doi.org/10.1021/jacs.8b04520.

Hahn, M.W., Steib, M., Jentys, A., Lercher, J.A., 2015. Mechanism and kinetics of CO_2 adsorption on surface bonded amines. J. Phys. Chem. C. 119, 4126–4135. https://doi.org/10.1021/jp512001t.

Yu, J., Chuang, S.S.C., 2017. The role of water in CO_2 capture by amine. Ind. Eng. Chem. Res. 56, 6337–6347. https://doi.org/10.1021/acs.iecr.7b00715.

Sayari, A., Liu, Q., Mishra, P., 2016. Enhanced adsorption efficiency through materials design for direct air capture over supported polyethylenimine. ChemSusChem 9, 2796–2803. https://doi.org/10.1002/cssc.201600834.

Kumar, D.R., Rosu, C., Sujan, A.R., Sakwa-Novak, M.A., Ping, E.W., Jones, C.W., 2020. Alkyl-aryl amine-rich molecules for CO_2 removal via direct air capture. ACS Sustain. Chem. Eng. 8, 10971–10982. https://doi.org/10.1021/acssuschemeng.0c03706.

Elfving, J., Bajamundi, C., Kauppinen, J., Sainio, T., 2017. Modelling of equilibrium working capacity of PSA, TSA and TVSA processes for CO_2 adsorption under direct air capture conditions. J. CO2 Util. 22, 270–277. https://doi.org/10.1016/j.jcou.2017.10.010.

Goeppert, A., Czaun, M., May, R.B., Prakash, G.K.S., Olah, G.A., Narayanan, S.R., 2011. Carbon dioxide capture from the air using a polyamine based regenerable solid adsorbent. J. Am. Chem. Soc. 133, 20164–20167. https://doi.org/10.1021/ja2100005.

Wang, J., Huang, H., Wang, M., Yao, L., Qiao, W., Long, D., Ling, L., 2015. Direct capture of low-concentration CO_2 on mesoporous carbon-supported solid amine adsorbents at ambient temperature. Ind. Eng. Chem. Res. 54, 5319–5327. https://doi.org/10.1021/acs.iecr.5b01060.

Sujan, A.R., Pang, S.H., Zhu, G., Jones, C.W., Lively, R.P., 2019. Direct CO_2 capture from air using poly(ethylenimine)-loaded polymer/silica fiber sorbents. ACS Sustain. Chem. Eng. 7, 5264–5273. https://doi.org/10.1021/acssuschemeng.8b06203.

Qi, G., Fu, L., Giannelis, E.P., 2014. Sponges with covalently tethered amines for high-efficiency carbon capture. Nat. Commun. 5, 1–7. https://doi.org/10.1038/ncomms6796.

Si, W., Ye, S., Zhang, D., Yang, B., Hou, Y., Li, Z., Zhang, X., Zhu, J., Lei, L., 2019. Kinetics and mechanism of low-concentration CO_2 adsorption on solid amine in a humid confined space. Can. J. Chem. Eng. 97, 697–701. https://doi.org/10.1002/cjce.23257.

Kolle, J.M., Fayaz, M., Sayari, A. Understanding the effect of water on CO2 adsorption (accepted), Chem. Rev. Article ASAP. https://doi.org/10.1021/acs.chemrev.0c00762.

Wang, Z., Goyal, N., Liu, L., Tsang, D.C.W., Shang, J., Liu, W., Li, G., 2020. N-doped porous carbon derived from polypyrrole for CO_2 capture from humid flue gases. Chem. Eng. J. 396,. https://doi.org/10.1016/j.cej.2020.125376 125376.

Stampi-Bombelli, V., van der Spek, M., Mazzotti, M., 2020. Analysis of direct capture of CO_2 from ambient air via steam-assisted temperature–vacuum swing adsorption. Adsorption 26, 1183–1197. https://doi.org/10.1007/s10450-020-00249-w.

Jung, W., Lee, K.S., 2020. Isotherm and kinetics modeling of simultaneous CO_2 and H_2O adsorption on an amine-functionalized solid sorbent. J. Nat. Gas Sci. Eng. 84,. https://doi.org/10.1016/j.jngse.2020.103489 103489.

Elfving, J., Kauppinen, J., Jegoroff, M., Ruuskanen, V., Järvinen, L., Sainio, T., 2021. Experimental comparison of regeneration methods for CO_2 concentration from air using amine-based adsorbent. Chem. Eng. J. 404,. https://doi.org/10.1016/j.cej.2020.126337 126337.

Elfving, J., Bajamundi, C., Kauppinen, J., 2017. Characterization and performance of direct air capture sorbent. Energy Procedia. 114, 6087–6101. https://doi.org/10.1016/j.egypro.2017.03.1746.

Do, D.D., 1998. Adsorption analysis: Equilibria and kinetics. Imperial College Press.

Serna-Guerrero, R., Belmabkhout, Y., Sayari, A., 2010. Modeling CO_2 adsorption on amine-functionalized mesoporous silica: 1. A semi-empirical equilibrium model. Chem. Eng. J. 161, 173–181. https://doi.org/10.1016/j.cej.2010.04.024.

Wang, Y., LeVan, M.D., 2009. Adsorption equilibrium of carbon dioxide and water vapor on zeolites 5A and 13X. J. Chem. Eng. Data. 54, 2839–2844. https://doi.org/10.1021/je800900a.

Qasem, N.A.A., Ben-Mansour, R., 2018. Adsorption breakthrough and cycling stability of carbon dioxide separation from $CO_2/N_2/H_2O$ mixture under ambient conditions using 13X and Mg-MOF-74. Appl. Energy. 230, 1093–1107. https://doi.org/10.1016/j.apenergy.2018.09.069.

Sultan, M., El-Sharkawy, I.I., Miyazaki, T., Saha, B.B., Koyama, S., Maruyama, T., Maeda, S., Nakamura, T., 2015. Insights of water vapor sorption onto polymer based sorbents. Adsorption. 21, 205–215. https://doi.org/10.1007/s10450-015-9663-y.

Quirijns, E.J., Van Boxtel, A.J.B., Van Loon, W.K.P., Van Straten, G., 2005. Sorption isotherms, GAB parameters and isosteric heat of sorption. J. Sci. Food Agric. 85, 1805–1814. https://doi.org/10.1002/jsfa.2140.

Sonnleitner, E., Schöny, G., Hofbauer, H., 2018. Assessment of zeolite 13X and Lewatit® VP OC 1065 for application in a continuous temperature swing adsorption process for biogas upgrading. Biomass Convers. Biorefinery. 8, 379–395. https://doi.org/10.1007/s13399-017-0293-3.

Bollini, P., Brunelli, N.A., Didas, S.A., Jones, C.W., 2012. Dynamics of CO_2 adsorption on amine adsorbents. 1. Impact of heat effects. Ind. Eng. Chem. Res. 51, 15145–15152. https://doi.org/10.1021/ie301790a.

Shafeeyan, M.S., Daud, W.M.A.W., Shamiri, A., 2014. A review of mathematical modeling of fixed-bed columns for carbon dioxide adsorption. Chem. Eng. Res. Des. 92, 961–988. https://doi.org/10.1016/j.cherd.2013.08.018.

Haghpanah, R., Majumder, A., Nilam, R., Rajendran, A., Farooq, S., Karimi, I.A., Amanullah, M., 2013. Multiobjective optimization of a four-step adsorption process for postcombustion CO_2 capture via finite volume simulation. Ind. Eng. Chem. Res. 52, 4249–4265. https://doi.org/10.1021/ie302658y.

Rastegar, S.O., Gu, T., 2017. Empirical correlations for axial dispersion coefficient and Peclet number in fixed-bed columns. J. Chromatogr. A. 1490, 133–137. https://doi.org/10.1016/j.chroma.2017.02.026.

Sircar, S., Hufton, J.R., 2000. Why does the linear driving force model for adsorption kinetics work? Adsorption. 6, 137–147. https://doi.org/10.1023/A:1008965317983.

Farooq, S., Ruthven, D.M., 1990. Heat effects in adsorption column dynamics. 2. Experimental validation of the one-dimensional model. Ind. Eng. Chem. Res. 29, 1084–1090. https://doi.org/10.1021/ie00102a020.

Miller, D.D., Yu, J., Chuang, S.S.C., 2020. Unraveling the structure and binding energy of adsorbed CO_2/H_2O on amine sorbents. J. Phys. Chem. C. 124, 24677–24689. https://doi.org/10.1021/acs.jpcc.0c04942.

Alkhabbaz, M.A., Bollini, P., Foo, G.S., Sievers, C., Jones, C.W., 2014. Important roles of enthalpic and entropic contributions to CO_2 capture from simulated flue gas and ambient air using mesoporous silica grafted amines. J. Am. Chem. Soc. 136, 13170–13173. https://doi.org/10.1021/ja507655x.

Lee, J.J., Yoo, C.J., Chen, C.H., Hayes, S.E., Sievers, C., Jones, C.W., 2018. Silica-supported sterically hindered amines for CO_2 capture. Langmuir. 34, 12279–12292. https://doi.org/10.1021/acs.langmuir.8b02472.

Sinha, A., Darunte, L.A., Jones, C.W., Realff, M.J., Kawajiri, Y., 2017. Systems design and economic analysis of direct air capture of CO_2 through temperature vacuum swing adsorption using MIL-101(Cr)-PEI-800 and mmen-Mg_2(dobpdc) MOF adsorbents. Ind. Eng. Chem. Res. 56, 750–764. https://doi.org/10.1021/acs.iecr.6b03887.

Bollini, P., Brunelli, N.A., Didas, S.A., Jones, C.W., 2012. Dynamics of CO_2 adsorption on amine adsorbents. 2. Insights into adsorbent design. Ind. Eng. Chem. Res. 51, 15153–15162. https://doi.org/10.1021/ie3017913.

Serna-Guerrero, R., Sayari, A., 2010. Modeling adsorption of CO_2 on amine-functionalized mesoporous silica. 2: Kinetics and breakthrough curves. Chem. Eng. J. 161, 182–190. https://doi.org/10.1016/j.cej.2010.04.042.

Darunte, L.A., Sen, T., Bhawanani, C., Walton, K.S., Sholl, D.S., Realff, M.J., Jones, C.W., 2019. Moving beyond adsorption capacity in design of adsorbents for CO_2 capture from ultradilute feeds: Kinetics of CO_2 adsorption in materials with stepped isotherms. Ind. Eng. Chem. Res. 58, 366–377. https://doi.org/10.1021/acs.iecr.8b05042.

Ruthven, D.M., 1984. Principles of adsorption and adsorption processes. Wiley.

Bos, M.J., Kreuger, T., Kersten, S.R.A., Brilman, D.W.F., 2019. Study on transport phenomena and intrinsic kinetics for CO_2 adsorption in solid amine sorbent. Chem. Eng. J. 377,. https://doi.org/10.1016/j.cej.2018.11.072 120374.